3-22-2012

Methane Dual Expander Aerospike Nozzle Rocket Engine

Michael D. Moen

METHANE DUAL EXPANDER AEROSPIKE NOZZLE ROCKET ENGINE

THESIS

Michael D. Moen, Capt, USAF

AFIT/GA/ENY/12-M12

DEPARTMENT OF THE AIR FORCE
AIR UNIVERSITY

AIR FORCE INSTITUTE OF TECHNOLOGY

Wright-Patterson Air Force Base, Ohio

AFIT/GA/ENY/12-M12

METHANE DUAL EXPANDER AEROSPIKE NOZZLE ROCKET ENGINE

THESIS

Presented to the Faculty

Department of Aeronautics and Astronautics

Graduate School of Engineering and Management

Air Force Institute of Technology

Air University

Air Education and Training Command

In Partial Fulfillment of the Requirements for the

Degree of Master of Science in Astronautical Engineering

Michael D. Moen, B.S.

Captain, USAF

March 2012

AFIT/GA/ENY/12-M12

METHANE DUAL EXPANDER AEROSPIKE NOZZLE ROCKET ENGINE

Michael D. Moen
Captain, USAF

March 2012

Approved:

_____	_____
Carl R. Hartsfield, Lt Col, USAF (Chairman)	Date
_____	_____
Richard E. Huffman, Lt Col, USAF (Member)	Date
_____	_____
Ronald J. Simmons, Lt Col, USAF (Member)	Date
_____	_____
Richard K. Cohn, USAF (Member)	Date

Abstract

The Air Force Institute of Technology (AFIT), working to meet requirements set by the Air Force Research Laboratory's Next Generation Engine (NGE) initiative, is developing upper stage rocket models. The current path of investigation focuses on combining a dual expander cycle with an aerospike nozzle, or the Dual Expander Aerospike Nozzle (DEAN) using methane fuel. The methane DEAN (MDEAN) design process will rely heavily on AFIT's previous work, which focused on the development of tools for and the optimization of a liquid hydrogen/liquid oxygen DEAN engine. The work outlined in this paper expands the existing research by substituting liquid methane for liquid hydrogen. The targets derived from the NGE program include a vacuum specific impulse of 383 seconds, 25,000 lb_f of thrust, and a thrust to weight ratio of 108. Additionally, although no quantifiable requirements are provided, reliability and reusability are identified as design priorities. NASA's Numerical Propulsion System Simulation (NPSS^{TM}) was used in conjunction with Phoenix Integration's ModelCenter^{TM} to optimize over several parameters to include O/F ratio, thrust, and engine geometry. After thousands of iterations over the design space, the selected MDEAN engine concept has 349 s of I_{sp} and a thrust to weight ratio of 120. The MDEAN was compared to liquid hydrogen technology, existing methane technology, and the NGE goals.

Acknowledgments

I would like to thank my thesis advisor, Lt. Col Hartsfield, who has put great effort in discussing, teaching, and encouraging my progress through the AFIT program. Jay Simmons consistently applied his programming expertise and positive attitude towards figuring out complicated problems and for that I thank him. I thoroughly enjoyed working with him and value his keen insight and tireless energy. I thank Lt. Col Simmons for his expertise using NPSS; he taught me how to better think about using the tool. Many thanks to Dr. Cohn from the Air Force Research Laboratory for being on my committee and for fostering collaboration across two great organizations. Thanks to Lt. Col Huffman for serving on my committee. Finally to my fiancé, family, and friends, thank you for supporting me through this research and listening to me constantly talk about thermodynamics.

Michael D. Moen

Table of Contents

Page

List of Figures

Page

Page

List of Tables

Page

Page

METHANE DUAL EXPANDER AEROSPIKE NOZZLE ROCKET ENGINE

I. Introduction

The US Air Force is increasingly reliant on capabilities provided through platforms located in the space domain. Mission areas currently include functions vital to the joint force such as intelligence, surveillance and reconnaissance, command and control, navigation, weather, counterspace, and communications [1]. Spacelift, the mission area by which the AF gains access to the space domain, relies on chemical rocketry. Access to the space domain is predicated on achieving a change in velocity of approximately 7.8 km/s for low Earth orbit and an additional change in velocity specific to the desired location of the asset. Chemical rocketry is currently the only viable technique for attaining the required launch velocity change and therefore warrants continued study in search of increased efficiency and reliability.

Fiscal constraints necessitate researching reliable, cost effective technologies that can meet national spacelift requirements. Though significant (on the order of $5,000 per lb) [2], the cost of space launch is a relatively small fraction of overall program acquisition cost. Therefore, the chief spacelift requirement is reliability. Following this logic, overall program costs must decrease given financial constraints, but the effort to save program funds through research and development of the space launch mission area must not decrease the likelihood of successful launch.

Requirements

A combined government/industry team developed targets for launch capability performance under the Next Generation Engine (NGE) program with the overarching

goal to reduce the cost of space launch. The program strives to advance the performance of existing technologies to better support launch capability and thereby decrease the overall cost of delivering assets to space. The goals of the NGE program important to the current research are the performance parameters pertaining to upper stage engines. To represent a significant improvement over the state of the art, the NGE has determined an upper staged engine will need a specific impulse, I_{sp}, of 383 seconds, 25,000 pounds (lb_f) of thrust, and a thrust to weight ratio of 108. Additionally, reliability and reusability are cited as requirements without specific quantifiable measures. The current research employs a Dual Expander Aerospike Nozzle (DEAN) concept to attempt to meet these requirements. It is important to note, while AFIT has looked to the NGE program as a source of research goals, AFIT is not associated with the other participants of the formal NGE program (financially or otherwise).

The DEAN Model

Past work has occurred at AFIT related to this subject matter. Thus far, a model was developed (see Figure 1) to characterize the performance of a hydrogen/oxygen DEAN upper stage rocket. The model was then upgraded and incorporated into ModelCenter™ (a commercial modeling tool) in an effort to automate parametric study of design variables. Another upgrade introduced a more realistic isentropic contour to the geometry and further refined the model. Current research seeks to leverage the exceptional work of the past AFIT team to create a more efficient hydrogen/oxygen modeling tool and subsequently convert it to operate with methane chemistry and fluid

properties. The previous efforts will be described in detail in the background chapter of this paper.

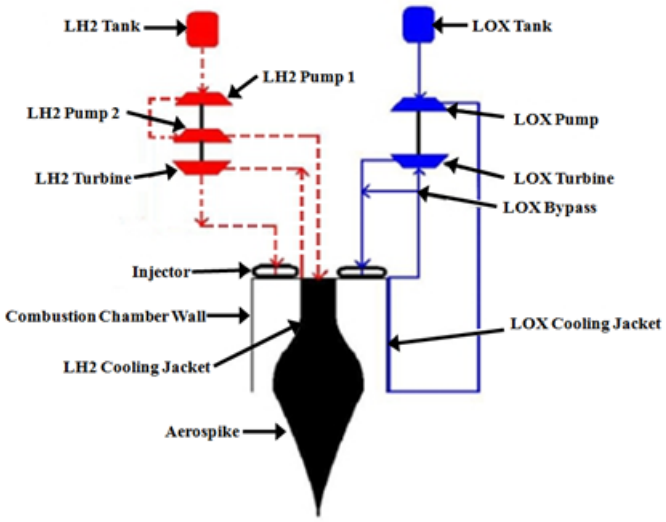

Figure 1: DEAN Schematic. From Hall, Inspired by Simmons.

The primary distinguishing characteristic of the new rocket design as compared to prior AFIT research is the replacement of cryogenic hydrogen fuel with cryogenic methane. For an ideally expanded rocket nozzle, I_{sp} varies directly with the rocket characteristic exhaust velocity. To maximize the exhaust velocity, the molecular weight of the exhaust products can be minimized through propellant selection, and because of its low molecular weight, hydrogen is an attractive propellant. Despite the performance advantage of hydrogen over methane, launch operations are complicated through the use of cryogenic hydrogen. Additionally, the foremost source (approximately 96%) of hydrogen is the processing of fossil fuel. Natural gas specifically accounts for about 29% of annual hydrogen gas production [3]. Advantages of cryogenic methane relative to

other options are examined in the background chapter of this paper and performance comparisons are made in the results chapter.

Research Objectives

Current research will support the NGE upper stage methane rocket performance goals through the following objectives:

1. Update the existing hydrogen/liquid oxygen DEAN Model with an emphasis on modularization and efficiency.
2. Update the existing DEAN Model with methane/liquid oxygen chemistry and fluid properties.
3. Perform parametric studies on the updated model.
4. Analyze the resulting design points against NGE performance goals and historical designs.

Multiple design tools will be employed to pursue the research objectives. ModelCenter by Phoenix Integration will control the input and results from multiple modeling tools. Additionally, ModelCenter has the capability of performing statistically relevant parametric studies of the DEAN design variables. NASA's Numerical Propulsion System Simulation (NPSS^{TM}) will calculate parameters for the various components of the rocket model. Finally, NASA's Chemical Equilibrium with Applications (CEA^{TM}) will be used for chemical data including fluid properties.

II. Literature Review

Background

The fundamental goal of this research is the development of a model that calculates performance parameters of a methane rocket employing a dual expander engine cycle and an aerospike nozzle. It will be shown whether performance peculiar to the chosen initial design options is appealing for continued development, provided there is an advantage in performance over existing concepts. This chapter examines rocket engine theory, previous DEAN research, the preliminary design decisions, and the basis for performance comparison.

Rocket Theory

Ideal Rocket Equation

The basis of the key performance parameter (I_{sp}) is derived from the transfer of momentum from the rocket to the rocket exhaust gases [4]. To derive the relationship between the task to be performed by the rocket (a change in velocity) and the change in mass of the rocket due to the consumption of propellant, external forces are neglected and the total momentum of the system is assumed to be static:

$$\frac{dP_{system}}{dt} = 0 \tag{1}$$

This suggests that any momentum that is removed from the rocket body is fully transferred to the exhaust, or the change in the momentum of the rocket is equal to the opposite the change in momentum of the exhaust.

$$(m - dm)dv = -dmv_e \tag{2}$$

The variable v_e is the exhaust velocity of the propellant exiting the rocket, and it defines the primary rocket performance parameter through the following relation.

$$v_e = I_{sp} g_0 \tag{3}$$

Simplifying these expressions results in an integral where m_i and m_f are the initial and final mass of the rocket, respectfully.

$$\int_0^{\Delta v} dv = -v_e \int_{m_i}^{m_f} \frac{dm}{m} \tag{4}$$

This reduces to

$$\Delta v = -v_e ln\left(\frac{m_f}{m_i}\right) \tag{5}$$

The final simplification is the substitution relating exit exhaust velocity to specific impulse:

$$\Delta v = -I_{sp} g_0 ln\left(\frac{m_f}{m_i}\right) \tag{6}$$

Now, given a specific mission (Δv), a rocket (I_{sp}) can be chosen that will provide the needed capability with an estimate of the necessary fuel ($m_i - m_f$). The challenge undertaken in this study is to calculate a reasonable estimate of I_{sp} for a specific rocket concept over a range of design variables.

Possible Mission Scenario and Requirements

Possible mission requirements are described by the NGE solicitation for an upper stage hydrogen rocket for the future replacement of the RL-10 [5]. The most basic rocket mission requirement is the translation of the mission into a quantifiable capability that leads to engineering decisions. In the case of an upper stage engine, a suitable starting point is the required Δv. For this effort, a common upper stage maneuver, a transfer from

a parking orbit (v_i = 7.79 km/s) to a geosynchronous orbit (v_f = 3.08 km/s), is taken as a baseline for a relevant Δv. As rocket propulsion has relatively high thrust, an impulsive transfer between the two orbits of interest with an inclination change of 28° at the apogee of the transfer orbit is used to calculate the Δv. The inclination change is included based on launching out of Cape Canaveral, FL. The first maneuver is calculated as a Hohmann transfer of 2.46 km/s. To calculate the scalar change in the velocity of the two maneuvers, the law of cosines is employed for the second maneuver.

$$\Delta v_B = \sqrt{\left(v_i^2 + v_f^2 - 2v_i v_f \cos\theta\right)} \tag{7}$$

$$\Delta v_{total} = 4.29\left({}^{km}/_{s}\right) = \Delta v_A + \sqrt{(1.59^2 + 3.08^2 - 2(1.59)(3.08)\cos(28))} \tag{8}$$

The overall mission associated with the upper stage must achieve a change in velocity of 4.29 km/s. The change in velocity will be used with the ideal rocket equation to determine if an engine with a given I_{sp} is suitable for the upper stage representative mission. A challenge with the conceptual development of useful rocket engines is the nature of the space enterprise. Because of the expense and the global reach of space assets, many payloads are unique. Each payload needs mission analysis to determine the proper propulsion solution, but the DEAN model development assumes a general mission. Although the current work doesn't fully support a rigorous systems engineering process, the goal is to develop a robust enough engine concept that the design will satisfy several different space lift missions, or at the very least, find an interesting niche for which it is particularly suitable.

The NGE solicitation provides additional requirements in the form of constraints for an upper stage hydrogen engine. Total thrust, F, is to be set at 25,000-35,000 lb_f [5].

Additionally, the thrust to weight ratio, T/W, is to be greater than or equal to 108, and I_{sp} must be greater than 465 seconds. While the NGE solicitation specifically identifies a hydrogen/oxygen cryogenic upper stage engine, it is still of interest to investigate the possibility of a methane rocket. NGE seeks methods to increase capability over a baseline, the RL10. The current work derived derives the MDEAN requirements from similar increases in performance over a different baseline, the RD-185, while keeping the basic functionality of providing 25,000 lb_f of vacuum thrust. The RD-185 has a vacuum I_{sp} of 378 and a thrust to weight ratio of 44 [6]. These baseline requirements will be used as input variables for parametric study, constraints for the design (thrust), or calculated output (I_{sp}, T/W). The NGE requirements are the criteria used to evaluate the performance of the MDEAN.

Engine Cycle

The characterization of the method of propellant transfer into the combustion chamber is known as the engine cycle (excluding the specifics of injection). Several engine cycle options exist for a cryogenic liquid rockets. The driving factors in the refinement of cycle selection are the range of pressurization necessary from the propellant tanks to the combustion chamber, geometry, complexity, sizing, and performance. Three engine cycles are more popular and have been demonstrated in mission capable designs. Diagrams of the three most popular cycles (gas generator, staged-combustion, and expander) can be found in Figure 2.

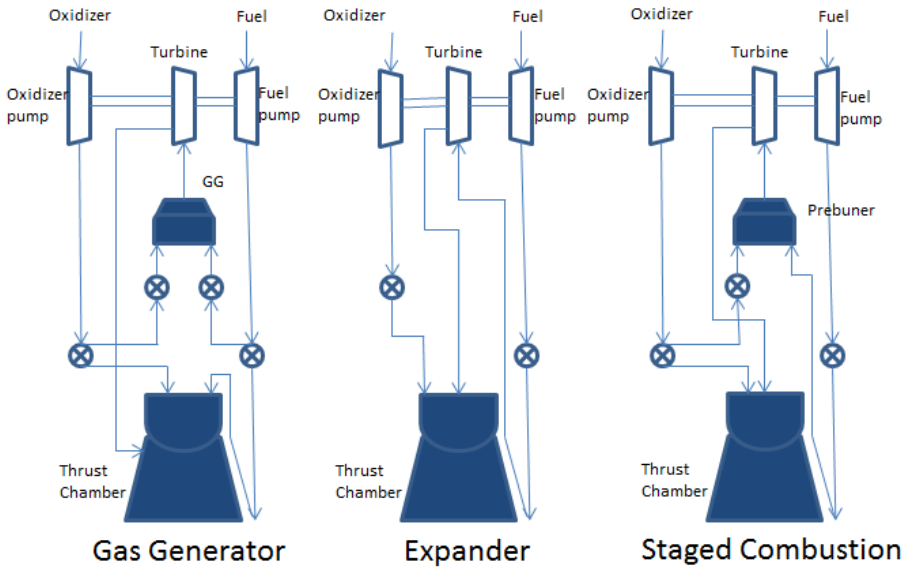

Figure 2: Common Rocket Cycles.

One top level distinction is the open system versus the closed system. The open cycle combusts a portion of the propellant flow to drive a turbine which in turn operates the fuel and oxidizer pumps. The products from the turbine are exhausted overboard, and this cycle concept is known as the gas-generator cycle. This cycle provides a comparatively simple solution to propellant pressurization at the cost of performance. For a given chamber pressure, the gas-generator cycle decreases overall engine I_{sp} by 2% to 5% [4]. The driving force for concept refinement in the early stages of DEAN was based on maximizing I_{sp} at a specific thrust and thrust to weight ratio. Because the goal of DEAN is high performance, the gas-generator cycle was not selected for modeling.

Closed cycles have greater opportunity to reach the high level of performance required by the NGE solicitation [4]. The two most common closed cycle concepts that are examined are the staged-combustion and the expander cycles.

The expander cycle flows propellants through a heat exchanger which cools the combustion chamber and nozzle. The coolant is traditionally the fuel which absorbs heat and drives a turbine which operates the fuel and oxidizer pumps. All of the unreacted propellant then enters the combustion chamber and is expanded through the nozzle. The DEAN design concept differs from the traditional expander cycle in its dual nature. The DEAN flows both the fuel and oxidizer through heat exchangers and each flow independently powers the fuel and oxidizer pumps. Overall system weight is reduced when compared to the other cycles because there is no gas generator or extra combustion chamber providing energy to the turbo machinery. Additionally, the organization of the regenerative cooling system associated with the cycle has a synergistic match with the geometry inherent to an aerospike layout. The layout of the engine plumbing is therefore simplified to an extent, and the likelihood of fuel and oxidizer interaction outside the combustion chamber is reduced. The probability of this known failure mode is therefore reduced, theoretically increasing the reliability of the overall rocket system.

The staged combustion cycle, as seen in Figure 2, has a similar flow to the expander cycle in that the propellants travel through a heat exchanger which is linked to the combustion chamber and nozzle. After the propellants are heated, a portion flows into a pre-burner combustion chamber that consumes the flow of fuel and some of the flow of oxidizer. The products of this combustion operate a turbine to power the propellant pumps and then flow into the primary combustion chamber. The primary advantage of the staged combustion concept is the high achievable chamber pressure which will lead to a high performance engine [7]. The primary disadvantage is the volume, complexity, and mass of the extra combustion equipment. Although this cycle

would conceivably work for the DEAN, the chosen mission scenario of upper stage space launch favors a smaller, simpler concept. The ideal design concept will be small enough to fit within the confines defined by existing hardware, not to exceed 90 inches in length with a diameter not to exceed 73 inches [5].

Therefore, having eliminated the performance drop of the gas generator and the bulk of the staged combustion cycles, the DEAN concept incorporates an expander cycle. The additional design feature of the dual expander system takes advantage of the aerospike geometry and will ease plumbing design.

Turbo machinery

Turbo machinery refers to the turbines and pumps that make up the expander cycle of the DEAN. This system of equipment is highly tuned to a specific rocket design and provides propellants at the proper pressure, temperature, and mixture ratio to drive the combustion process in the chamber at the design flow rate. The primary advantages of using turbopumps in a rocket engine concept is their capability to provide high combustion chamber pressures with lower propellant storage tank pressures. Both of these conditions tend to decrease the overall mass of the engine concept. Lower pressure tanks can have thinner walls due to lower hoop stress. A higher chamber pressure can equate to a volumetrically smaller, potentially lighter chamber with improved performance.

Pressure Budget

To begin the sizing process for the turbopumps, the pressure drop across the system must be estimated [4]. The estimation process outlined by Humble *et al*. starts with the desired chamber pressure and steps through the pressure losses through the

system in reverse order: chamber pressure, injector, turbine, cooling jacket, pumps, propellant tanks. For an initial estimate, the pressure drop across the injector is estimated at 20% of chamber pressure at normal operating conditions or 30% of chamber pressure for throttled operation. This pressure drop is due to one of the injector's primary functions, the isolation of propellant flow perturbations between the chamber and the feed system [4]. The next step is to assume a pressure ratio across the turbine. Humble *et al*. estimates a turbine pressure ratio of 1.5 for an expander cycle [4]. Hall estimated a pressure ratio of 1.84 for the oxidizer and a pressure ratio of 1.56 for the hydrogen fuel [8]. Based on historical data, Humble *et al*. recommend a cooling jacket pressure drop of 15% of chamber pressure [4]. The associated dynamic pressure drop can be estimated by Bernoulli's equation:

$$\Delta p = \frac{1}{2}\rho v^2 \tag{9}$$

The velocity can be assumed to be about 10 m/s and a piping diameter can be based on equation 10, calculated from the pipe cross sectional area, A_{pipe}. As with equation 9, ρ is density and v is velocity.

$$\dot{m} = \rho v A_{pipe} \tag{10}$$

By assuming a reasonable storage tank pressure, the required pressure increase due to pumping can be calculated. A ratio of note, the pressure ratio, is the required pressure entering the cooling jacket divided by the storage tank pressure. This ratio will be used in an engine balance.

Engine Balance

The pressure rise provided by the pumps corresponds to a power. The energy imparted to the flow through the pumps must be balanced through the energy imparted to the turbine and through the thermal energy captured through the cooling jacket. The balance starts by setting the required pump power equal to the power of the turbine [4] while assuming a constant specific heat over the range of encountered temperatures:

$$p_{req} = \frac{g_0 \dot{m} H_p}{\eta_p} \cong \eta_T \dot{m}_T C_p T_i \left[1 - \left(\frac{1}{p_{trat}} \right)^{\frac{\gamma - 1}{\gamma}} \right] \tag{11}$$

where

p_{req} = Power required to drive the pump

g_0 = Acceleration due to gravity (m/s^2)

$\dot{m}$ = Mass flow rate (kg/s)

H_p = Pump head rise (m)

η_p = Pump efficiency

η_T = Turbine efficiency

C_p = Constant pressure specific heat (J/kgK)

γ = Isentropic parameter

T_i = Turbine inlet temperature (K)

p_{trat} = Turbine pressure ratio

For the DEAN concept, each turbine must be balanced against the corresponding pump(s). The turbine inlet temperature must be determined based on the energy imparted to the propellants through the walls of the cooling jacket. The solution must be found through iteration until the powers match to within acceptable tolerance.

Existing Work

The existing design provided by Martin includes two turbopump assemblies which were developed by Arguello [9] and Strain [10] specifically for the DEAN.

Because the development of turbomachinery specifications is laborious, this research leaves specific component selection and/or development to future research. Based on model development, reasonable pressure ratios will be assumed for the turbomachinery and specific calculated changes in propellant state will be checked for viability. Past work has developed calculated efficiencies for liquid oxygen and liquid hydrogen turbomachinery. The change over from hydrogen to methane will significantly change the design of the turbopump. The fuel with higher density, methane, will require less head and therefore less power [7]. This will reduce the size of the pump assembly for the methane fueled rocket, saving mass.

Combustion Chamber

The combustion (or thrust) chamber is the heart of the rocket where the chemical energy of the propellants is converted into thrust (see Figure 3). The propellants are atomized through the injector so the resulting droplets are quickly vaporized. Then the combustion of the gaseous propellants increases the temperature and the flow rate. The combustion products flow is then accelerated through a nozzle to supersonic velocities prior to ejection [11]. The process heats and accelerates the propellants and can generate an extreme environment of high pressures and temperatures which the combustion chamber must survive for the duration of the mission. The added qualitative goals of reusability and reliability increase the need for the chamber to resist deformation or failure during operation over multiple cycles. Increased resilience can be attained

through a higher margin of safety for load calculations which will result in thicker walls or exploration into stronger materials.

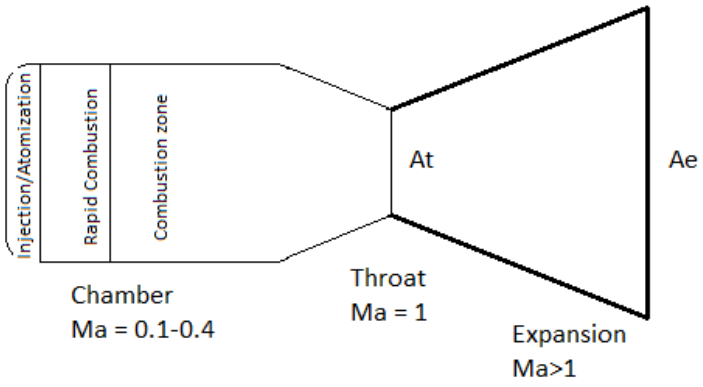

Figure 3: Thrust Chamber.

Performance Measures

An important quantitative measure of a thrust chamber is the characteristic velocity, c^*. It will be shown later (equations 26 through 28) that c* is proportional to the primary rocket measure of performance, I_{sp}.

$$c^* = \frac{p_c A_t}{\dot{m}} = \frac{\eta_{c^*}\sqrt{\gamma R T_c}}{\gamma\left(\frac{2}{\gamma+1}\right)^{\frac{\gamma+1}{2\gamma-2}}} \tag{12}$$

c^* is dependent on the components of the product gas at the exit of the chamber. Once a propellant has been chosen, every variable will be set (within a range) in the above equation except for the temperature. The characteristic velocity then mostly depends on the temperature, which should be maximized to the extent feasible. Too high a temperature will weaken the chamber walls, causing failure due to the extreme forces

involved with the high pressures. For methane and oxygen, an estimated c^* to start engineering estimates is 6020 ft/s [7].

Another important measure of the chamber-nozzle pair is the thrust coefficient, C_f, which represents the gas expansion performance through the nozzle and is defined as the force generated with the expansion through the nozzle over the force due to the pressure over the area of the throat alone, or:

$$C_f = \frac{F}{A_t p_c} \tag{13}$$

where

F = Thrust (lb_f)

A_t = Throat Area (in^2)

P_c = Chamber Pressure (psia)

Combustion chamber sizing

One possible goal in designing the layout of the combustion chamber is to ensure complete combustion prior to acceleration through the nozzle portion of the chamber. Any unreacted propellant exiting the combustion chamber represents a loss of potential energy and a decrease in the conversion of chemical energy into thrust. This phenomenon is complicated by the possibility of incomplete combustion providing a lower average molecular weight of the combustion products, which also increases performance. The characteristic length is related to the completeness of combustion in a chamber and is defined as:

$$L^* = \frac{V_c}{A_t} \tag{14}$$

where

L^* = Characteristic Length (in)

V_c = Chamber Volume (in^3)

A_t = Throat Area (in^2)

L^* is the length a chamber (of equal volume) would have if it was a straight tube without the converging nozzle section. An early estimate for a methane rocket characteristic length can be derived from the ranges of values found in Humble *et al* [4]. A cryogenic hydrogen/oxygen rocket can range from 0.76 to 1.02 meters. An RP-1 /oxygen rocket can range from 1.02 to 1.27 meters. Larger L^* can cause system level performance degradations by increasing size and weight of the chamber, increasing the surface area requiring cooling, and increasing frictional losses in the chamber [12].

The residence time is a measure of the mean length of time a molecule spends in the reactor [12],

$$t_R = \frac{\rho V_c}{\dot{m}} \tag{15}$$

L^* relates to the residence time through

$$L^* = \frac{V_c}{A_t} = \frac{\dot{W} V_c t_R}{A_t} \tag{16}$$

The residence time depends on the chemical kinetics of the reacting species and is determined experimentally. The residence time can vary between 0.0001 and 0.040 seconds for different types and sizes of chamber [7]. As the characteristic length of a chamber increases, the volume of the chamber will increase, the velocity of the propellants will decrease and the residence time will increase. There is an opportunity for exploration of the thermo chemistry with this relationship and L^* is therefore an input design variable for the MDEAN. For the MDEAN modeling effort, the L^* design

variable exploration will begin in the neighborhood of one meter, the high end for a hydrogen rocket and the low end of an RP-1 rocket.

Nozzle

The performance measures most important to the NGE program are specific impulse (I_{sp}), thrust (F), and the thrust to weight ratio (T/W). While the rocket as a whole must be considered to calculate these values, the equations used to calculate them are largely centered on the characteristics and states defined by the chamber and the nozzle. The I_{sp} was defined with the development of the ideal rocket equation as being directly proportional to the velocity of the combustion products at the exit of the nozzle. Another representation is as a ratio of the thrust to the propellant mass flow rate, or

$$I_{sp} = \frac{F}{\dot{m} g_0} \tag{17}$$

This equation describes I_{sp} as a measure of the total performance of the rocket. It is the generated kinetic thrust imparted to the rocket per mass flow rate of the propellant. A useful analogy to this relation would be the fuel economy of an automobile, or miles per gallon.

The nozzle accelerates and ejects combustion products to impart momentum to the rocket. Thrust is generated by a rocket through two mechanisms, momentum thrust and pressure thrust [4]. Total momentum of the system is conserved at zero, so as the fluid accelerates and exits the rocket, the rocket builds momentum equally but in the opposite direction creating momentum thrust. Pressure thrust is created as the pressure exiting the rocket, p_e, can be unequal to the ambient pressure, p_a. With one-dimensional, steady flow through the nozzle, there will only be a pressure differential in the direction

of propellant flow. Pressure differentials in other directions will be equal and opposite due to the symmetry of the rocket and therefore cancel. The basic thrust equation then becomes:

$$F = momentum\ thrust + pressure\ thrust \tag{18}$$

$$F = \dot{m}v_e + (p_e - p_a)A_e \tag{19}$$

As the gas exits the combustion chamber, it enters into the nozzle and is accelerated to Mach 1. After passing through the throat, the gas is further accelerated through the divergent portion of the nozzle and decreases in temperature and pressure as thermal energy is converted to kinetic energy. The process over the length of the nozzle is complicated as the thermodynamic properties are dependent on the constantly changing state of the gas. Several different assumptions can aid in the calculation of the state through the nozzle.

The first possible simplification for the flow through the nozzle is the condition of frozen composition. The assumption asserts that the composition of the flow remains constant through the expansion of the nozzle. There are no chemical reactions or phase changes. To restate, the composition at the exit of the nozzle is identical to the composition for the chamber condition. This assumption is chosen for simplicity of calculation and because the resulting performance estimates are conservative. Frozen flow calculations underestimate performance by one to four percent [11]. The frozen flow assumption will be primarily utilized through the calculations of gaseous properties provided by CEA.

Equilibrium flow is more complex and assumes the products constantly shift during the expansion portion of the nozzle. The equilibrium is modeled to exist between chemical composition and phase. This more complex assumption results in inflated calculations for I_{sp} or c* and is therefore not used in the DEAN [11].

The final, unused assumption attempts to model the equilibrium flow to include the reaction rates of the steps between the multiple equilibrium states. The complexity of the calculation combined with the lack of sufficient data on the rates of the assumed reaction mechanisms usually prevent this type of calculation.

Aerospike

The aerospike nozzle has several advantages over a conical nozzle and was therefore incorporated in the initial design considerations. The development of the calculations to determine aerospike performance is explored in chapter 3.

Conical approximation

For the purpose of this study, the contour of the aerospike nozzle will be treated as conical. Previous DEAN work demonstrated that the conical aerospike developed reasonable approximations for mass calculations while significantly decreasing processing time. Specifically, conical approximations vary by less than 10% [8] from calculations based on the more complex contours. Therefore, to save computational time and operate with streamlined, easily testable and modifiable code, Hall's recommendation of using a conical nozzle contour will be implemented in the current work.

Truncation

Previous DEAN work (the first DEAN model) explored the impact of truncating the aerospike nozzle downstream of the throat. The conclusion was that I_{sp} didn't vary significantly with nozzle length and the truncation provided savings to the mass of the engine. A truncation of 25% resulted in a reduction of 8.5% of the mass of the nozzle [13]. Reduction of the supersonic expansion section of the nozzle of up to 75% only reduced modeled I_{sp} by 1.6%. From Martin's work, it can be concluded that a modest truncation of 25-50% should result in a lighter engine with slightly lower performance.

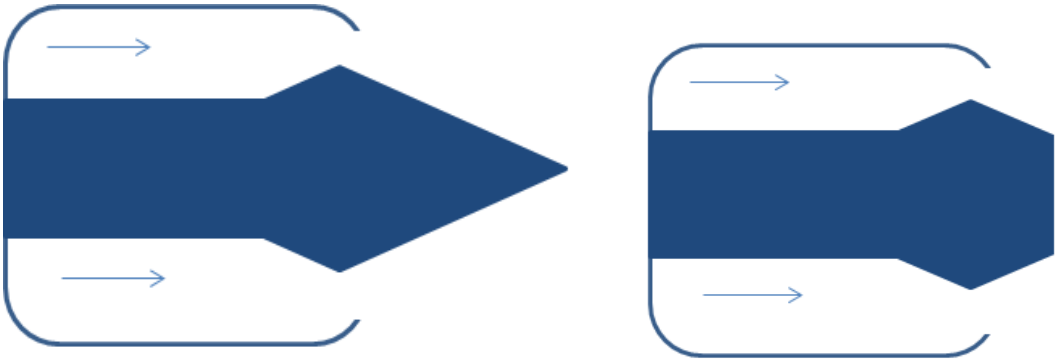

Figure 4: Conical Aerospike vs. Truncated Conical Aerospike.

The truncation of the optimized 3rd generation DEAN model further demonstrated that within a regime of up to 50% truncation (see Figure 4), performance is not significantly reduced [8]. Hall's model estimated performance loss of approximately 0.83% for 49% nozzle truncation. Truncation beyond this length impacted the expander cycle portion of the cooling jacket that is located on the nozzle. Significant decreases in performance occur beyond 80% truncation. Based on the changes in performance and mass, Hall concludes any change in the truncation of the nozzle must be considered in the

context of a full stage design [8]. A shorter, lighter, lower performing engine might be the appropriate choice, if the remainder of the rocket can reach mission objectives. It is possible to significantly reduce the overall length of the aerospike nozzle while avoiding significant impact to the overall performance.

Cooling Jacket Theory

The rocket works by transferring chemical energy into useful propulsive energy in the combustion chamber. To reach this condition, the pressure and temperature of the propellants must be correct for efficient combustion. In the DEAN concept, a regenerative cooling expander cycle removes energy from the combustion chamber and nozzle and uses that energy to transport and pressurize the propellants from the storage tanks to the injector and chamber. The cooling function prevents hardware failure due to weakening from high temperature and transfers that energy to the working fluids via the turbomachinery. It is important to understand how the energy moves through the system so that realistic modeling of the performance of the rocket can be understood. Energy is conducted through the walls of the combustion chamber to the cooling jacket and then is imparted to the heat exchanger working fluids, the propellants, via convection.

The first method of transfer of thermal energy is convection from the hot combustion gases to the walls of the combustion chamber and nozzle. The basic equation to model this heat transfer is [7]:

$$\dot{q} = h_g\left(T_{aw} - T_{wg}\right) \tag{20}$$

where

$\dot{q}$ = Heat flux (Btu/in^2)

h_g = Gas-side heat transfer coefficient (Btu/(in^{2}R))

T_{aw} = Adiabatic wall temperature of the gas (R)

T_{wg} = Hot gas side local chamber wall temperature (R)

The challenge in this development then becomes the estimation of the heat transfer coefficient. The empirical relation developed by Bartz is used to estimate h_g. This estimate is one of the largest sources of error for the rocket model development and is on the order of ten to twenty percent [7].

$$h_g = \left[\frac{0.026}{D_t^{0.2}}\left(\frac{\mu^{0.2}C_p}{Pr^{0.6}}\right)_{ns}\left(\frac{(p_c)_{ns}g}{c^*}\right)^{0.8}\left(\frac{D_t}{R}\right)^{0.1}\right]\times\left(\frac{A_t}{A}\right)^{0.9}\sigma \tag{21}$$

where

D_t = Throat diameter (in)

C_p = Constant pressure specific heat (Btu/lb °F)

Pr = Prandtl number = $\mu C_p/k$

μ = viscosity (lb/in s)

R = Nozzle radius of curvature at throat (in)

σ = Correction factor for property variations over boundary layer

A = Area along chamber axis (in^2)

Similarly, the thermal energy is then imparted to the propellants through convection through the cooling jacket walls. Again, the challenge with the problem is estimating the heat transfer coefficient, now h_c for the cold side. Concern must be given to the phase of the coolant liquids. If the pressure of the fluid is below the critical pressure, limited vaporization can occur as nucleate boiling, that is, a vapor bubble will form in the liquid and grow until it is constrained by the rate of condensation at the edge

of the bubble. The heat flux into the cooling liquid can increase tremendously with a relatively small increase in the coolant side wall temperature over the nucleate boiling regime, but there is an upper limit of heat flux at which too many bubbles will form and cause the coolant side wall temperature to dramatically increase, usually causing structural failure. The upper boundary of nucleate boiling can therefore be used as a practical design boundary.

If the cooling fluid is above the critical pressure, no boiling can occur. Although the high rate of heat flux associated with nucleate boiling is attractive, the initial design choice of an expander cycle indicates supercritical pressures are needed to avoid condensation in the turbomachinery. With the operating regime selected as supercritical pressures, the empirical relation, the Sieder-Tate equation for turbulent flow can be used to approximate h_c.

$$h_c = \frac{0.029 C_p \mu^{0.2}}{Pr^{2/3}} \left(\frac{G^{0.8}}{d^{0.2}}\right) \left(\frac{T_{co}}{T_{wc}}\right)^{0.55} \tag{22}$$

where

G = Coolant weight flowrate per unit area (lb/in^2 s)

d = Coolant passage hydraulic diameter (in)

T_{co} = Coolant bulk temp (R)

T_{wc} = Coolant side wall temperature (R)

The total cooling capacity of the regenerative cooling system can be estimated as:

$$Q_c = \dot{w}_c C_p (T_{cc} - T_{ci}) \tag{23}$$

where

Q_c = Coolant capacity (Btu/s)

$\dot{w}_c$ = Coolant mass flow rate (lb/s)

T_{cc} = Coolant critical temperature (R)

T_{ci} = Coolant inlet temperature (R)

Oxygen and methane critical point data is presented in Table 1.

Table 1: Propellant Critical Point Data.

Propellant	Critical Temperature (R)	Critical Pressure (psia)
Oxygen	278.26	731.425
Methane	343.62	672.927
Hydrogen	59.76	188.108

The total amount of energy removed from the chamber and imparted into the propellants is an important performance parameter where hydrogen has a major advantage over methane due to heat transfer characteristics. In the updated methane DEAN model, it will be necessary to verify that the modeled heat transfer rate, Q is safely less than Q_c as calculated above.

The transfer of thermal energy from the inner wall of the combustion chamber to the inner wall of the cooling jacket involves conduction. Conductive heat transfer is defined by Fourier's Law [4]:

$$\dot{Q} = -kA\frac{dT}{dx} \tag{24}$$

where

$\dot{Q}$ = Rate of heat transfer (Btu/s)

K = Thermal conductivity (Btu/(ft*s*R))

A = Cross sectional area perpendicular to flow (in^2)

T = Temperature (R)

x = Distance in direction of heat flow (in)

At every step (chamber to wall, through the walls, wall to coolant), the rate of heat transfer is the same, so it is possible to calculate the wall temperatures based on material properties. The desirable characteristics of the material for the wall are high thermal conductivity and a high maximum possible operating temperature. Additionally, high pressures found in the cooling channels and the chamber drive structural requirements of the hardware, dictating the thickness of walls.

Small passages with high flow rates and high pressures lead to large pressure drops which are a drain on the efficiency of the design and should therefore be minimized. Therefore, the pressure drop across the channels is dependent on plumbing layout. Changes in direction and contractions and expansions must be minimized. The pressure drop can be calculated by:

$$\Delta p = f \frac{L}{d} \frac{\rho V_{co}^2}{2g} \tag{25}$$

where

Δp = Pressure drop (lb/in^2)

L = Length of the portion being measured (in)

d = Equivalent average diameter (in)

ρ = Average coolant density (lb/in^3)

V_{co} = Coolant flow velocity (in/s)

g = Mass conversion factor (in/s^2)

f = Friction loss coefficient

Materials

As noted earlier, the combustion process creates extreme environments which can cause failures through multiple mechanisms. The different elements of the engine must survive the associated stresses with an appropriate safety margin (1.5 for the DEAN [8]). High temperatures can cause structural weakness and the combustion chamber and nozzle must be able to withstand high pressures while held at high temperatures. The cooling channels must survive highly pressurized, reactive fluid streams. The turbomachinery is exposed to the corrosive fluids and thermal gradients. To attain the reusability and reliability required by the NGE proposal, all structures must remain below material limits with margins of safety. Martin's material choices were chosen based on processes only reaching 50% of melting points [13]. Additionally, Martin accounted for material compatibility with the propellants of liquid hydrogen and liquid oxygen. The cooled section of the aerospike was copper and the tip was made of niobium. Silicon carbide comprised the cooled section of the chamber while the jacket was made of aluminum.

Upon more detailed investigation into the optimization of thrust to weight, Hall selected materials to meet the NGE goals and ease manufacturability [8]. Oxygen free copper was selected for all of the aerospike components. The chamber again used silicon carbide because of the favorable thermal properties. To avoid reaction with the propellants, the hydrogen plumbing was made from INCOLOY 909 and the oxygen plumbing was made from INCONEL 718.

Previous Work

Martin

David Martin used NASA's NPSS to design the first DEAN model, which is built up through different elements, each representing the different components of the rocket design [13]. Martin's methodology assumed rocket engine parameters based on historically successful designs and used NPSS to perform a power balance and a pressure budget. NPSS validated the reasonableness of the initial estimates and calculated more accurate parameters. Once the model solution closed, Martin explored design changes to increase performance.

Martin's objectives were to explore the feasibility of meeting the NGE research goals with the hydrogen DEAN concept, establish a design process focused on the energy conversion sections of the rocket, and to perform detailed design analysis of energy transfer components. The results in Table 2 demonstrate that the DEAN design was an excellent candidate for further study in pursuit of the NGE goals.

Table 2: Martin's DEAN Design

	DEAN	DEAN Goals	Comparison
Vacuum Thrust (lb_f)	57,231	50,000	+14.5%
Vacuum I_{sp} (s)	472	464	+1.7%

Additionally, Sierra Engineering's software package Two Dimensional Kinetics (TDK'04™) was used to develop the aerospike geometry. TDK'04 used combustion chamber data (pressure and temperature) to develop the nozzle contour. Further work explored performance loss from aerospike truncation, with the goal of volume and weight savings. The result of this analysis was that significant truncation of the nozzle (up to

50%) past the throat resulted in minor decreases (on the order of 2%) in system performance.

Simmons

Joseph Simmons upgraded the DEAN model with a focus on automation of parametric studies [14]. The goal of the work was to develop the tools necessary to optimize the thrust to weight ratio of the DEAN model, and this was accomplished through adding geometry parameters into the model and exploring the O/F ratio. The result was a more robust DEAN modeling tool that produced a design with similar performance, but a significantly shorter, and therefore lighter, engine. To accomplish this, the NPSS independent variables and dependent conditions were adjusted. The NPSS model was wrapped in ModelCenter for greater control and automation. The input and output variables of NPSS were therefore readily available for study and additional analysis.

Simmons' work extracted top level parameters from the inner workings of the DEAN model to make them available for parametric evaluation. For example, before Simmons' work, the O/F ratio was controlled indirectly through manipulating pump pressure ratios. By reallocating the O/F ratio as a design variable, Simmons increased performance by decreasing the O/F ratio from 7 to 6, thereby finding an optimum value for this engine and cycle. An optimum O/F ratio increases the amount of energy that can be harnessed from the combustion reaction and therefore may yield increased performance, provided chamber and throat temperatures stay within material temperature limits. The expander cycle active cooling of the surfaces in question should allow for this increase in performance, and the DEAN model checks for these limits through energy

balances and material property checks. The ModelCenter controlled NPSS model produces a closed design for each set of input parameters so geometries, chamber pressures, etc. may all change between designs; for this reason it was important to reorganize the input and output variables.

The end result of the effort was the development of a more accurate model with an increase in the number of customizable user inputs. The automation of the parametric analyses provides the user with the ability to quickly create a family of rocket engines at various discreet, closed designs. The generated designs can then be analyzed for desired characteristics. Using Martin's design input characteristics, the new design process developed an engine with the following performance.

Table 3: Simmons' Parametric Results.

	Initial DEAN	**DEAN - v2**	**Requirements**
Vacuum Thrust (lb_f)	57,231	50,000	50,000
Vacuum Isp (s)	472 s	464	464
O/F	7	6	N/A
Mass Flow (lb_m/s)	121	104	N/A
Length (in)	37.2	27.9	N/A

Hall

Hall used the updated ModelCenter/NPSS DEAN design tool to develop a substantially more detailed system level design point through the use of automated trades and parametric studies [8]. Additionally, the reusability of the design was examined through a materials survey which provided material property data to the model. The temperature dependent material property data was incorporated into automated checks for structural integrity. Different sections of the engine experience different stresses and temperatures. The performance calculations Hall developed estimate the volumes of the

rocket components (and therefore mass) and check the resulting pieces against selectable failure criteria. The resulting design performance is listed in Table 4. Hall's additions to the design tool included much more accurate modeling of the aerospike nozzle behavior, including losses and reasonable expansion ratios. Additionally, Hall finalized the capability to analyze vacuum thrust-to-weight ratio, giving the modeling tools substantially more utility in the pursuit of the NGE requirements.

Table 4: Hall's DEAN Design Performance.

	DEAN - v3	DEAN Goals	Comparison
Vacuum Thrust (lb_f)	50,161	50,000	+0.3%
Vacuum T/W	142.2	106.5	+33.5%
Vacuum I_{sp} (s)	430.6	464	-7.3%

Preliminary Design Decisions

Dual Expander Cycle

Traditional single expander rocket systems use fuel flow, usually liquid hydrogen, to remove heat from the combustion chamber and nozzle. The heated fuel then flows through a turbine to provide mechanical work to the fuel and oxidizer pumps. The pumps pressurize the fuel and oxidizer for the combustion chamber injector system. The dual expander system differs in that both the fuel and oxidizer are used as working fluids; therefore the design includes a fuel expander cycle and a completely separate oxidizer expander cycle. By separating the two flow systems, the likelihood of failure due to fuel/oxidizer mixing prior to the combustion chamber is reduced. Also, the separation increases options for material selection for either feed system based on the material compatibility of the fluid. In addition, by using essentially the full mass flow of the engine to power the pumps, the pump pressure ratio can be increased and the turbine

pressure ratio decreased, permitting increased chamber pressure. Increased chamber pressure for a given propellant flow rate increases performance by lowering the area of the throat and all subsequently derived engine dimensions, cutting engine mass [4].

Aerospike Nozzle

The first advantage of the aerospike nozzle is geometry that is conducive to a dual expander design. Because the combustion flow occurs in an annular region, there are two separated surfaces available for heat transfer from the chamber into the pre-combustion working fluids. This separation should ease plumbing design and therefore lower total plumbing/fuel system weight. Savings would be realized in a specific stage design, which is beyond the scope of this project. Second, the aerospike nozzle can operate optimally at all altitudes of flight. Although this benefit seems of little consequence for an upper stage engine, developmental test and evaluation would be simplified. Because of the high cost of space systems acquisitions, space launch customers demand a rigorously tested launch solution. This design choice therefore has the potential to dramatically reduce the cost of test and evaluation of a launch acquisition by reducing the complexity of the required testing infrastructure, as all developmental testing could be done at local atmospheric conditions, requiring a low pressure chamber only for final verification testing.

Methane Fuel

Some properties of cryogenic methane are appealing when compared to hydrogen. The significantly higher boiling point temperature and the larger enthalpy of vaporization at the normal boiling point (NBP) imply that there could be a gain of efficiency on the pad waiting for launch (See Table 5). Hydrogen boil-off on the pad is estimated at 1.2%

per hour, requiring crews to "top off" launch vehicles near launch [15]. Less energy will be needed to keep the cryogenic fuel at an appropriate temperature, the rate of energy conduction into insulated tanks will be reduced (because of the smaller change in temperature), and the greater enthalpy of vaporization means there should be less boil off on the pad, reducing the extra fuel to be added in a design through engineering margin.

Table 5: Properties of Cryogenic Fuels [16].

Property	Unit	Hydrogen	Methane
Molecular Weight	g/mole	2.0159	16.043
Tb @ 1 atm or NBP	K	20.28	111.668
Enthalpy of Vap @ NBP	J/g	445	510.83
Liquid Density @ NBP	g/mL	0.0708	0.4224
Heat Capacity (l) @ NBP	J/gK	9.668	3.481

The combustion products of methane have a relatively low molecular weight. The chemical species of greatest abundance in methane/oxygen combustion products are H_2O, CO, H_2 , and CO_2 . The relative amount of product species depends on several factors to include combustion chamber geometry, temperature, and pressure [12]. In equations 26 through 28, it is shown that I_{sp} is inversely related to products molecular weight, MW [4]. While methane compares unfavorably with hydrogen, it compares favorably against many other fuels.

$$I_{sp} = \lambda \left\{ \frac{c^* \gamma}{g_0} \sqrt{\left(\frac{2}{\gamma - 1}\right)\left(\frac{2}{\gamma + 1}\right)^{\frac{\gamma+1}{\gamma-1}} \left[1 - \left(\frac{p_e}{p_c}\right)^{\frac{\gamma-1}{\gamma}}\right]} \frac{c^* \varepsilon}{g_0 p_c} (p_e - p_a) \right\} \tag{26}$$

$$c^* = \frac{\eta_{c^*} \sqrt{\gamma R T_c}}{\gamma \left(\frac{2}{\gamma + 1}\right)^{\frac{\gamma+1}{2\gamma-2}}} \tag{27}$$

$$R = \frac{8314}{MW} [=] \frac{J}{kg \cdot K} \tag{28}$$

Toxicity of combustion products is not terribly important for upper stage engines, but low toxicity lends itself to the development of a reusable, safe, and very testable device. When combined with the atmospheric compensation of the aerospike nozzle, the DEAN concept is relatively easy to test on the ground.

Basis of Comparison

Considerable work has been applied to the development of aerospike engines in the past, so it is important to note the performance of previous work to determine if current efforts provide a comparative advantage. The first opportunity for comparison is the previous work of Hall, a similarly derived DEAN with hydrogen fuel. Unfortunately, this will not quite provide a perfect comparison as Hall's requirements were somewhat different than what is currently being investigated. The different fuel will give the hydrogen based design a higher I_{sp} and total performance advantage, but the target of 50,000 lb_f [8] of thrust prevents a direct comparison.

Previous methane based engine concepts exist in the literature. Klepikov *et al*. present a variety of engines employing methane as fuel [6]. The first, RD-185 is an upper stage engine designed for use with methane. The second two, RD-167 and RD-160, are modifications of the kerosene engines, RD-134 and RD-161, respectfully. All three of these engines include bell nozzles with large area ratios. The performance parameters of several historical engines of interest are in Table 6.

Table 6: Comparable Engine Performance.

Engine	RD-185[6]	RD-167[6]	RD-160[6]	NGE – Derived	NGE[5]	H-DEAN[8]
Fuel	CH_4	CH_4	CH_4	CH_4	H_2	H_2
Thrust (lb_f)	40,344	79,366	4,409	25,000	25,000	44,694
I_{sp} (s)	378	379	380.6	383	465	429.8
T/W	44	63	15.5	108	N/A	142.2

III. Methodology

With research goals defined, this chapter describes the method by which the MDEAN model was developed. The chapter begins with a discussion of the different software tools used in the development and includes descriptions of some of the critical software functions necessary for model calculations. Next is a more focused description of how NPSS uses thermochemistry and an explanation on the development of the different fluid property tables. Finally, there is a discussion on the modifications to NPSS and ModelCenter that were necessary for the hydrogen to methane fuel conversion.

Tools

ModelCenter

ModelCenter by Phoenix Integration is a program designed for the development and study of software models. Many other programs can be "wrapped" by ModelCenter to control input and to accept and analyze output. A key feature is the automation of parametric studies, allowing for a large amount of untended software execution that is necessary to explore a design space. Additionally, ModelCenter has a design-of-experiments function that allows the user to statistically analyze the response of a system for efficient optimization of input design variables. The visualization suite provides a convenient method of displaying and analyzing data.

ModelCenter is the top level software tool used to control the command line driven modeling programs, but it also has several features that have aided in the development and execution of the DEAN. A deeper level of automation and control of the NPSS model can be realized through the use of ModelCenter's included scripting

tools. Both VBScript and JavaScript were used in the DEAN models to perform intermediate calculations and provide functionality checks on the model. Additionally, the data import function allows a user to import data sets for analysis. The RMS toolkit can then be used to provide a polynomial or Kriging regression of data sets. The MDEAN primarily uses Kriging regression functions for thermodynamic tables based on enthalpy, which will be discussed in detail later.

Kriging Estimator

The Kriging function is a method of interpolation which relies on the observation of surrounding data points weighted for spatial covariance [17]. This method of the linear regression estimator, Z*(u) is defined:

$$Z^*(u) - m(u) = \sum_{\propto=1}^{n(u)} \lambda_\alpha [Z(u) - m(u_\alpha)] \tag{29}$$

where

u, u_α = location vector for estimation point and neighboring points with index α

n(u) = number of neighborhood points used for Z*(u) estimation

m(u), $m(u_\alpha)$ = expected mean values of Z(u) and $Z(u_\alpha)$

$\lambda_\alpha(u)$ = Kriging weight; each estimated $Z(u_\alpha)$ will have a different weight

The Kriging weight, λ_α, is the key to this method of estimation and is assigned to neighboring data points to find an estimate at the queried point u. The derivation to calculate the weights and an example can be found in reference [17]. The weight of a point often decreases as the distance from the location (temperature and pressure for the purposes of the MDEAN) to be estimated and that point increase. The ModelCenter Kriging function handles all calculations for the user, but care must be taken in the data

selection used in the Kriging generation. As with all interpolation algorithms, evenly spaced data covering all of the dataset to be analyzed will provide the best results. Step sizes must be small enough to provide ample coverage of non-linear behavior (or simply fast changing behavior), but the ModelCenter algorithm indicates best results occur with fewer than one thousand data points, so there is a tradeoff between step size and accuracy. Because the Kriging function is a weighted average, it will often produce estimates that are very smooth, sometimes more so than the actual data [17]. Another characteristic of this algorithm is that it should provide exact results if a data point used in Kriging generation is then queried with the function. This makes sense as the data point would be given a weighting to the exclusion of other points. Although it is positive that the Kriging can perfectly estimate some discreet data points, this phenomenon increases the workload with regards to error analysis as more source data is required to check the error of the Kriging generated estimates.

Polynomial Regression

In addition to Kriging interpolation, ModelCenter provides a polynomial regression tool to develop models for data sets. The polynomial regression is another method of linear regression, but the result is a polynomial function that approximates the shape of the input data. While the fit of this regression was usually lower than the Kriging, as evidenced by R^2 values, the method proved useful for developing one three dimensional fluid property table. The polynomial function is advantageous because it can be used directly in the place of the interpolation table. This is convenient as it eliminates the error from the linear interpolation. Unlike the Kriging, the polynomial function doesn't exactly predict the input data, so error analysis can largely be done with

the input data. Also, this linear regression can accommodate significantly more data, so error can be reduced in areas of interest by adding input data.

Numerical Propulsion Simulation System (NPSS)

NPSS is a NASA developed simulation program used to model engines and provide estimates of performance and is at the heart of the DEAN model. While NPSS was originally developed for air breathing applications, rocket based elements have been developed as of release 1.65 and the iterative solution methodology of the program lends itself to solving rocket systems.

Elements

NPSS works by combining elements that are mathematical representations of unit operations or physical phenomena. The NPSS Rockets Supplement [18] lists the relevant input and output variable names and units. Each element is an independent file of software which can be found in the InterpComponents directory under the NPSS installation directory (for version 1.65). Examining this code is helpful for understanding the underlying equations that are calculated by the solver. Some elements, such as the combustion chamber, have independent variables and dependent conditions associated with them which will be utilized for the overall system solver if the solver auto setup function is employed. Independent variables and dependent conditions are discussed below.

Ports

Ports are the software method by which elements are linked and include fluid ports, heat flow ports, or mechanical energy ports. Each element will have ports that must be connected to the ports of the other elements to provide the flow of mass or

energy. The linkPorts function builds the network of connections required by the iterative solver. A port is a software linkage and does not represent a physical connection. A fluid port does not include an associated pressure drop due to frictional losses. It is therefore necessary to include an element that has a frictional pressure loss to represent the physical fluid connection. That element (Valve04 in DEAN) will have at least two ports which must be linked to other elements.

Solver

The NPSS solver is an iterative algorithm which attempts to satisfy dependent conditions through the adjustment of independent variables. The goal of the solver is to drive the system model to a consistent, converged state. Several elements have built in independents/dependents and are usually associated with the fundamental continuity equations that are to be expected of a flow system. For example, mass flow entering an element is equal to mass flow exiting the same element. It is inevitable a model will require a controlling variable or condition that is not inherent in the comprising elements, so a user can add independent variables and dependent conditions. Independent variables and dependent conditions are associated with the system's solution method and therefore can only be added in pairs, unless the existing variables/conditions are modified, i.e. there need to be an equal number of independents and dependents so the solver can work with a square matrix.

The dependent conditions are organized as an equation, left hand side = right hand side (in the example above, mass flow in = mass flow out). Each side of this equation is dependent on one or more of the independent variables. For the sake of this development, consider each side being dependent on the independent variable x. The

inequality defines an error term which is equal to the difference of the two sides of the equation, but this simple error term is undesirable as the tolerance can then be variable amongst the different equations/dependents. For example, if each side of the dependent equation drives to a value of 1, a tolerance of 10^{-5} might be appropriate, but if each side of the dependent equation is driving to 10,000, then the same tolerance might be too restrictive [19]. Therefore, the error term is equal to the difference of the two sides of the equation divided by a reference term, which should be the same order of magnitude as the calculated solution to the equation. A quasi-Newton method is then used to drive the error term to zero. This means that the error term is calculated at the guessed value of the independent variable, x, and then the derivative of the error term curve is calculated at the guessed value of interest of x. This derivative at x forms a line that is propagated to where the error term is zero, and the value of x is found at this point. The process begins again along the error curve for the new value of x. The quasi nature of this method means the true slope is not calculated for every iteration in an effort to save computation time. This process is conducted amongst all independent/dependent interactions via a matrix known as the Jacobian. The Jacobian matrix is updated after a number of iterations via Broyden's method, which is explained in the NPSS User's Guide [19].

Output

As stated before, NPSS uses C++ syntax and therefore uses the *cout* command to print data. The cout function is used extensively in the MDEAN model to output the required NPSS output variables to a text file for review by a user or ModelCenter. A limitation of the *cout* command with regards to NPSS is it only prints converged,

successful runs or the final state before run failure. A different data dump function would be useful to see the evolution of an iterating run.

Chemical Equilibrium with Applications (CEA)

CEA is a NASA developed program used to calculate thermodynamic properties at different states. The primary use of CEA for the current work is for the calculation of thermochemical properties of the combustion products [20]. The CEA rocket problem function has several options which are set to specify the rocket parameters most desirable for the modeling application. For example, the DEAN combustion products are modeled by specifying the chamber state (pressure and temperature), the type of equilibrium (frozen flow), the O/F ratio, and the reactants (methane and oxygen). CEA assumes an ideal gas for the equation of state of the mixture of chemical species found in the reaction products. Chemical equilibrium is then defined by the minimization of free energy.

The following mathematical derivation is from the CEA guide, NASA Reference Publication 1311 [21]. Gibb's energy per kilogram mixture for NS species is given by equation 30 where n_j is the number of kilogram-moles of species j per kilogram of mixture:

$$g = \sum_{j=1}^{NS} \mu_j n_j \tag{30}$$

And μ_j, the chemical potential per kilogram-mole of species *j* is:

$$\mu_j = \left(\frac{\partial g}{\partial n_j}\right)_{T,P,n_{i+j}} \tag{31}$$

The equilibrium condition is described by the constrained minimization of the Gibb's energy, the constraint being a mass balance for the element *i*, or

$$\sum_{j=1}^{NS} a_{ij} n_j - b_i^0 = 0 \; (i = 1, \ldots, l) \tag{32}$$

where the first term is the number of kilogram-atoms of element *i* per kilogram of mixture (the number of element *i* atoms in molecule *j*) and b is the assigned number of kilogram-atoms of element *i* per kilogram of total reactants (total number of atoms of element *i*). The index *l* is the number of chemical elements. This constrained minimization problem is solved via Lagrange multipliers with the following definition:

$$G = g + \sum_{i=1}^{l} \lambda_i \left(\sum_{j=1}^{NS} a_{ij} n_j - b_i^0 \right) \tag{33}$$

λ_i are the Lagrange multipliers. The method of Lagrange multipliers is an optimization technique to find a local maxima or minima subject to constraints, the constraint being the mass balance. The equilibrium conditions are then calculated by:

$$\delta G = \sum_{j=1}^{NS} \left(\mu_j + \sum_{i=1}^{l} \lambda_i a_{ij} \right) \delta n_j + \sum_{i=1}^{l} (b_i - b_i^0) \delta \lambda_i = 0 \tag{34}$$

And as the variations are independents:

$$\mu_j + \sum_{i=1}^{l} \lambda_i a_{ij} = 0 \quad (j = 1, \ldots, NS) \tag{35}$$

This set of equations can then be solved for equilibrium concentrations with knowledge of the chemical potentials, μ_j [21].

NPSS Thermochemistry

NPSS supports a number of chemical species to include hydrogen and oxygen, but methane and its combustion products are not directly supported. There are several methods of incorporating thermodynamic data into the DEAN model, and each different method is specified in the model with the setThermoPackage command. The first method explored was direct integration of CEA calls into the NPSS code. When a calculation requires thermodynamic data, NPSS can launch CEA and acquire the necessary information. Unfortunately, the employed rocket elements were developed with unreacted fluid stations and therefore cannot make use of the CEA thermodynamics package. After consulting with Wolverine Ventures, the decision was made to develop custom fluid property tables for the chemical species of interest. A fluid property table includes several thermodynamic properties, each as a function of the state of the fluid and can be seen in Table 7 [22].

Table 7: Fluid Property Table Supported Parameters.

Property	**Unit**	**Property**	**Unit**
Density	lbm/ft3	Viscosity	lbm/(ft*sec)
Enthalpy	Btu/lbm	Thermal Conductivity	Btu/(sec*ft*R)
Internal Energy	Btu/lbm	Ratio of Specific Heats	N/A
Entropy	Btu/(lbm*R)	Prandtl Number	N/A
Const Vol Heat Cap	Btu/(lbm*R)	Molecular Weight	lbm/lb-mole
Const Press Heat Cap	Btu/(lbm*R)	Total Gas Constant	Btu/(lbm*R)

For the liquid propellants, the National Institute of Standards and Technology (NIST) thermodynamic database was used as the source of data [23]. Data was taken over the ranges of interest for methane and oxygen with ranges and step sizes determined through logical analysis of the problem at hand. For both propellants, the phase of the

chemical species dictated the area of interest for thermodynamic data. Methane and Oxygen exist in the rocket as pure species from the propellant tanks to the injector and should only exist as liquids or supercritical fluids because vapor would cause flow instabilities and possible cavitation in turbo-machinery. The phase data of the pure propellants therefore partially dictate the ranges of temperatures and pressures at which data should be tabulated. Below, Figure 5 shows the boiling temperatures of methane over a range of pressures. This curve represents the lower boundary of the query for NIST data. Below the indicated pressure, the pure chemical is a gas and is therefore not applicable to the fluid flow problem.

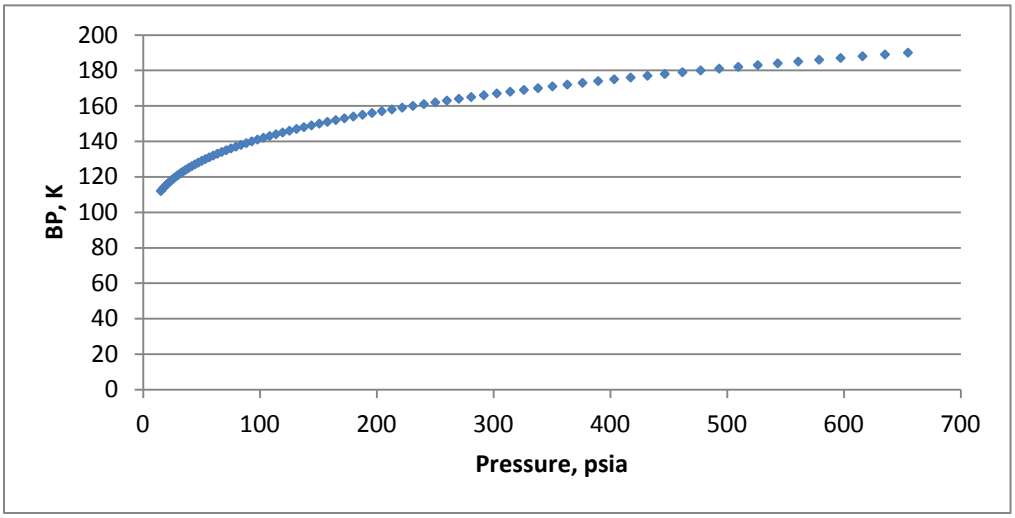

Figure 5: Methane Boiling Point Temp vs. Pressure (Antoine Equation).

NIST includes very high pressure data for both oxygen and methane with upper limits being 11,893 psia and 145,037 psia respectively. For the purposes of the DEAN, the upper boundaries for the fluid property tables are significantly reduced based on historical data. First, the upper end of chamber pressures for Hall's designs is approximately 3000 psia [8]. Accounting for an approximate 30% [4] pressure drop for

an injector and a 20% drop for a turbine sets a reasonable upper pressure bound of 4600 psia for all propellants. For margin, the tables were extended to 6000 psia in the supercritical region. If a fluid station has a state beyond the limits of the table, NPSS will extrapolate a value for a queried property. This represents a possible source of error and should be avoided if at all possible.

The temperature limits used for the fluid property tables are outlined in Table 8. The low temperature was set at a convenient integer slightly above the species melting point at one atmosphere. This value was chosen because frozen propellants are undesirable and will not occur in the DEAN model by design. The NIST database upper temperature limits are 1125 Rankin for methane and 1800 R for oxygen [23]. The tables include high temperature data up to the NIST limit in an attempt to eliminate error from extrapolation. One mode by which the NPSS model failed to converge was due to the oxygen temperature exceeding the upper temperature limit of the fluid property table. The extrapolation method was set to *Lagrange2* at the time and NPSS returned a C_p of approximately -0.5. This caused the heat transfer coefficient on the cooling channel side to be a complex number (via the Bartz estimate, see equation 21) and NPSS was unable to continue calculation. The temperature range of the oxygen FPT was then expanded to the extent NIST provides and the extrapolation method was changed to linear for all tables.

Table 8: Fluid Property Input Data Independent Variable Ranges.

	Methane	**Oxygen**
T_{low} (R)	165	100
T_{high} (R)	1115	1800
P_{low} (psia)	15	15
P_{high} (psia)	6000	5000

The NPSS User's Guide [19] dictates the fluid property table syntax. For a given temperature (or enthalpy or entropy), a pressure sweep and the corresponding tabulated thermodynamic properties are listed. This organization dictates attempting to record significant pressure sweeps at discreet temperatures. Fortunately, the NIST database allows the setting of range and step size for data queries. The interpolation method for the fluid property tables is linear. This limitation/feature implies a requirement for the step size of the collected data. Over the ranges of the fluid properties that are linear, a large step size can be used. Over ranges where nonlinear behavior is observed (near the critical point), a smaller step size is needed to reduce interpolation error.

Methane FPT Generation

Based on the FPT example built with the NPSS Rocets thermodynamic package, the methane fluid property table requires the following individual property tables:

Table 9: Properties Required for Methane FPT.

Property, NPSS Symbol	Unit	Independent Variables	Indeps Call
Density, rho	lb_m/ft^3	h, P	N/A
Internal Energy, u	Btu/lb_m	h, P	N/A
Entropy, s	$Btu/lb_m/R$	h, P	N/A
Viscosity, mu	$lb_m/ft/s$	h, P	N/A
Const V Specific Heat, C_v	$Btu/lb_m/R$	h, P	N/A
Const P Specific Heat, C_p	$Btu/lb_m/R$	h, P	N/A
Thermal Conductivity, k	Btu/s/ft/R	h, P	N/A
Ratio of Specific Heats, gam	N/A	h, P	N/A
Temperature, T_h	R	h, P	ThIndeps
Enthalpy, h_T	Btu/lb_m	T, P	hTindeps
Temperature, T_s	R	s, P	TsIndeps
Enthalpy, h_s	Btu/lb_m	s, P	hsIndeps
Total Gas Constant, R	$Btu/lb_m/R$	h, P	N/A

The final column of the table, *Indeps* Call, refers to a command that is required before a table in the file. This command defines the independent variables to be used to define the state of the corresponding table/property. Every parameter marked N/A is handled by the first *indeps* call that specifies enthalpy and pressure as the two independent variables by which the tables are organized. The four parameters that have the *indeps* call field in the preceding table require an additional call before that particular parameter table is instantiated. Note the case sensitive nature of the command, enthalpy as a function of temperature and pressure has a lower case "i" in the *indeps* command. The format of the call is described in the NPSS thermodynamics reference sheets [22] and an example is:

```
hTindeps = {"Tt", "Pt"};
```

Enthalpy as a function of temperature and pressure was the easiest table to create as it is simply a reformatting of the raw NIST data. Data was collected from NIST and loaded into an Excel spreadsheet. In the spreadsheet, the data was organized by the independent variables and then it was wrapped into ModelCenter where the spreadsheet contents could be loaded into arrays. The arrays were then sent to a Visual Basic script where they were organized into the NPSS table format and output to a text file. The file was saved for future integration into the overall methane .fpt file.

The remaining tables divide into two groups, enthalpy based data and entropy based data. Two Kriging estimators were built based on those input variables. The process for building a Kriging model is to save the Excel data as tab delimited text data for easy import into ModelCenter using the data import function. Following the ModelCenter data import dialogue allows you to specify delimiter method, column

headings, columns for import, and input/output status of a parameter. Once the data is loaded with the appropriate specified input parameters (enthalpy and pressure or entropy and pressure), the RSM toolkit is launched so a Kriging model can be generated. The best results for the Kriging come from an even spacing of data over the entire range of interest and fewer than 1000 data points, which causes a tradeoff between data density and range coverage. The RSM toolkit provides some basic measures of quality for the Kriging estimator, an adjusted R^2 and a 1 to 5 star rating. The first attempt at Kriging resulted in less than adequate results.

Experimentation with the Kriging estimator led to a more complicated solution that reduced error and somewhat reduced the impact of the tradeoff between data density and range coverage. The data was divided by phase. This created four Kriging estimators to generate the remaining tables: the division of liquid versus supercritical and the basis of enthalpy or entropy as the independent variable. Additional data was taken for a more complete coverage of the range, all of the data was reorganized by phase, and the four Kriging estimators were generated. The change of the organization of the data from temperature to enthalpy as the independent variable caused some data in the range of the vapor phase to be included in the input data (the higher enthalpy input combined with the lower pressure input). No data in this range was included in the generation of the estimators so it is assumed that the Kriging provides incorrect data. Therefore, additional logic was included to eliminate the vapor phase data from the fluid property tables. The logic is explained below in the Rejection of Vapor Data section as the same method was included in the oxygen tables.

Enthalpy, entropy, and pressure input values are then organized into ModelCenter arrays and fed into the Kriging estimators in loops to get complete coverage of the input data ranges. Examining the first combination of enthalpy-based liquid data Kriging estimator as an example, the data generation process consists of an outer enthalpy loop with a nested pressure loop. This organization of data generation is based around the required NPSS table organization. In other words, for each input enthalpy, the inner loop calculates the Kriging estimate of each thermodynamic parameter for each specified pressure. The output from the Kriging estimator is a single value of each thermodynamic property of the data type double. The output doubles are stored in arrays of doubles by the "Pressure For Each Loop" component. Because ModelCenter passes arrays from component to component in the form of arrays of strings, some additional scripting was required to organize the data before preparing it for output. A Javascript component converts the array of doubles into a string. The single string for each property includes n values of each parameter where n is the number of input pressures. The enthalpy For Each Loop then collects each string into an array of strings. Therefore, after all input data is processed through the Kriging estimator, for each parameter, an array of strings exists, one string for each value of input enthalpy. Each string contains the n parameter values calculated based on the input pressure values.

This process is repeated four times, once for each Kriging estimator. The result is four string arrays that are already organized in the manner required by the NPSS table syntax. The data has to be organized monotonically within a table for all input variables. Care must be taken to avoid overlapping enthalpy values when using multiple Kriging estimators for one table. The phase change boundary provided a straight forward

demarcation of the input data, but overlap and resulting non-monotonic tables could be an issue when creating multiple Krigings without the clear demarcation. An output file is generated using the proper syntax and the string data is placed properly in the table.

The total gas constant is a constant for the pure chemical species and was therefore provided as a function rather than a table. The previously developed enthalpy as a function of pressure and temperature table must be added to the final fluid property table file. A future upgrade could include the integration of the different table generation techniques.

Oxygen FPT Generation

The Oxygen fluid property table generation process was very similar to the methane table generation except for a few complications. First, more data was available, so the temperature/enthalpy data range is significantly larger than that of the methane table. Additionally, the constant pressure specific heat as a function of enthalpy and pressure in the super critical phase Kriging estimator was of low quality. The ratio of specific heats was predictably also poor (see equation 38). Temperature data was generated based on enthalpy and pressure input into the Kriging estimator and the definition of constant pressure specific heat was employed via a numerical derivative.

$$C_p = \left(\frac{\partial H}{\partial T}\right)_P \tag{36}$$

The numerical derivative was taken by sorting the oxygen NIST data by pressure, and then calculating the partial derivative via equation 37 [24].

$$C_P]_x = \left(\frac{H_{x+1} - H_{x-1}}{T_{x+1} - T_{x-1}}\right) \tag{37}$$

The C_p values at the edges of each grouping of constant pressure data were then queried and supplied directly from the NIST database [23]. Data points near the critical point and near the boiling point were also directly supplied from NIST to reduce error. The Excel file was then wrapped in ModelCenter to save the different columns of data into arrays. The arrays were then output to text in the appropriate NPSS table syntax. The ratio of specific heats was simply included in the fluid property table as a function by its definition:

$$\gamma = {}^{C_P}/_{C_V} \tag{38}$$

When gamma is queried by NPSS, the C_p and C_v at the given state will be found in the table and gamma will be calculated directly. The oxygen gamma function is listed below as an example of the format for a NPSS fluid property table function.

```
real gam (real ht, real Pt) { return (Cp(ht,Pt)/Cv(ht,Pt));
```

Oxygen tables from all three sources must then be manually combined into one fluid property table file. The input sources are the master table created from the four Kriging estimators, the enthalpy as a function of temperature and pressure table generated directly from the NIST data, and the independently, spreadsheet generated constant pressure specific heat table.

Rejection of Vapor Data

NIST data on fluid properties is supplied as a function of temperature and pressure. NPSS needs the data organized as a function of enthalpy and pressure. In creating the fluid property tables, NIST data was captured and the vapor phase of methane and oxygen were excluded prior to Kriging estimator generation. After the data

was reorganized by an enthalpy basis, the input ranges of enthalpies and pressures were an easily organized matrix of values based on phase boundaries, executed with nested for loops. This presents a problem because the new enthalpy pressure input data ranges include regions that are vapor, and additionally, because of the exclusion of vapor data in the original sampling, the data is rendered meaningless as it does not represent the reality of the phase transition. The solution was to eliminate data outside of the ranges of the phase boundaries. The Antoine equation allowed for the elimination of any vapor phase data where P is the vapor pressure in bar, T is temperature in kelvin, and A, B, and C are the Antoine parameters. Given a temperature, the liquid will have a corresponding vapor pressure.

$$log_{10}(P) = A - \left(\frac{B}{(T + C)}\right) \tag{39}$$

The vapor pressure can also represent the pressure at which a fluid of temperature T will boil; therefore, this can be used as a relationship between pressure and boiling temperature. The output temperature of the Kriging functions was compared to the Antoine functions of the respective fluid. If the temperature was higher than the Antoine boiling temperature for a given pressure, the data was not retained for tabulation. In this way, vapor phase data in the new basis ranges was excluded from the enthalpy and entropy based fluid property tables.

Table 10: Antoine Coefficients for Oxygen and Methane.

Species	P - Unit	Temp Range (K)	A	B	C	Source
Oxygen	Bar	54.36 – 154.33	3.9523	340.024	-4.144	NIST [25]
Methane	Bar	90.99 – 189.99	3.9895	443.028	-0.49	NIST [26]

Combustion Products FPT Generation

The fluid property table for the combustion products is generated using NASA's chemical equilibrium with applications. The fluid property table was generated by controlling CEA with ModelCenter independent of NPSS because of the limitations of the unreacted fluid stations used in the rocket model elements. Because the oxygen to fuel weight ratio is a top level explored parameter, the combustion products fluid property table requires three independent variables (pressure, temperature, and OF) to define the combustion products thermodynamic state. Additionally, a reverse lookup table of temperature as a function of enthalpy, pressure, and OF is required per the NPSS Rockets Supplement [18].

NPSS thermochemical documentation is somewhat vague about how the program would interpret the data or whether O/F could even be used by the fluid station (O/F is not listed as a property supported by fluid property tables in the documentation, although it is a variable which can be queried at a fluid station). Therefore, it was decided to generate a unique combustion products fluid property table for every iteration of O/F. The appropriate FPT would have been generated before NPSS calculations and then called from NPSS by using ModelCenter to update the NPSS run file based on the O/F input. This solved the problem with the documentation ambiguity and should have reduced error by limiting the algorithm to two interpolations (temperature and pressure) rather than three interpolations. This method was abandoned when an example fluid property table for hydrogen/oxygen combustion products was generated using the NPSS Rocets database.

Ultimately, the chosen method was to generate a large three dimensional table which NPSS would linearly interpolate over three independent variables for gas properties. A ModelCenter program generated CEA input files for the rocket problem, and then captured the CEA output. The captured data was then organized and output into the proper NPSS fluid property table format.

The ranges of pressure and temperature for the combustion products FPTs were determined from historical examples found in an overview of rocket engine parameters by Oskar J Haidn [27]. From the listed rocket engines, the upper stage engines ranged in chamber pressure from 522 to 2147 psia. The overall range of liquid propellant rockets to include booster and main stage engines is 522 to 3698 psia. Additionally, the Russian RD-167 methane/lox rocket engine generates a chamber pressure of about 2500 psia [6]. The limits of the fluid property table for the combustion products will therefore be 15 psia to 4000 psia. Based on Hall's approximate highest chamber temperature, 7000 R [8], the range for the combustion products temperature independent variable will be 1000 R to 8000 R. The step size for both parameters will be small to reduce interpolation error. The step size for both temperature and pressure is the driver behind the error associated with the portion of this FPT that is based on temperature, pressure, and O/F.

The O/F ratios included in this table are based on CEA analysis using the Rocket problem. As expected, the optimum O/F ratio for methane and oxygen is at a significantly different ratio than hydrogen and oxygen and can be seen in Figure 6. CEA is used as a first look to determine a neighborhood of interest for the O/F parameter. The resulting vacuum I_{sp} is calculated based on only chemical and thermodynamic properties and has no system level dependence on energy or material transport. It is therefore only

used to examine relationships. Additionally, the calculated I_{sp} seen in Figure 6 is based on frozen flow conditions, and therefore represents a low estimate. The low number is not a concern as the input to CEA is not based on any optimization.

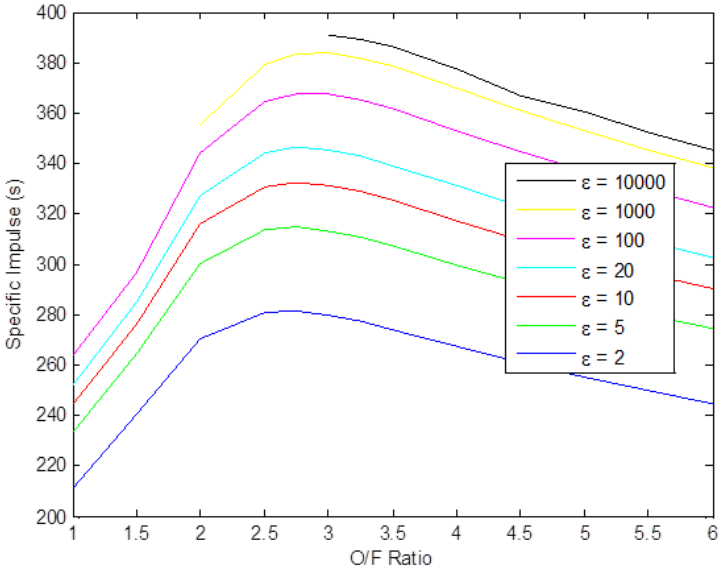

Figure 6: CEA I_{sp} vs. O/F at Various Expansion Ratios for CH_4/O_2, Frozen Flow.

Changing the expansion ratio has a significant effect on the specific impulse and the location of the optimum O/F ratio. Note the Hall hydrogen concept had an expansion ratio of 4.37. This first look shows that the area of interest for the current work should include O/F ratios from 2 to 5.

Temperature as a Function of Enthalpy, Pressure, and OF

Per the NPSS User's Guide [19] and the RocketComb1 Element [18], the fluid property table requires a reverse lookup table to find temperature as a function of enthalpy, pressure, and O/F. The first attempt at table generation used the method that was employed in the propellant tables, a Kriging interpolation that allowed for estimates of fluid properties to be organized by the different variables. For reasons discussed in the

results section, this was unsuccessful and error was significant. A new approach was attempted for this table, a three dimensional cubic polynomial. Significantly more data was used in the generation of the polynomial as compared to a Kriging generation which is limited to 1000 data points. Additionally, data density was increased in the range of interest where convergence is expected. The final polynomial employed in the model is in Table 11.

Table 11: Polynomial Approximation of Temperature as a Function of H, P, and OF.

Terms	Coefficients
Constant	6.6934E+02
O/F	3.4226E+03
Enthalpy	1.5122E+00
Pressure*Pressure	-3.0681E-04
O/F*O/F	-6.6019E+02
Enthalpy*Enthalpy	-1.2292E-04
Pressure*O/F	5.2064E-01
Pressure*Enthalpy	2.7619E-04
O/F*Enthalpy	-5.1952E-01
Pressure*Pressure*Pressure	4.8916E-08
O/F* O/F* O/F	3.5103E+01
Enthalpy*Enthalpy*Enthalpy	4.9080E-09
Pressure*Pressure*O/F	-2.5999E-05
Pressure*Pressure*Enthalpy	-3.8899E-08
Pressure*O/F*O/F	-5.5114E-02
Pressure*O/F*Enthalpy	-1.7437E-05
Pressure*Enthalpy*Enthalpy	-1.1080E-08
O/F*O/F*Enthalpy	6.1895E-02
O/F*Enthalpy*Enthalpy	9.2284E-06

This function is simply placed in the fluid property table in the proper format and returns a temperature when queried. The format is similar to the more simplistic gamma function described above.

Thermodynamic Reference State

Each source of data is defined by a different thermodynamic reference state. The NIST data defines the thermodynamic reference state as internal energy is equal to zero at 273.16 K for the saturated liquid [25, 26]. This also represents the enthalpy thermodynamic reference state per the definition of enthalpy [28]:

$$H = U + pV \tag{40}$$

This is true for each propellant. The combustion products data set is based on the CEA thermodynamic reference state, which is not directly and simply defined. For the purposes of the MDEAN, this is not necessary. The reference value is arbitrary because the change in enthalpy from one thermodynamic state to another is the important relation, and by the definitions of the thermochemical properties, a change from one thermodynamic state to another will represent the same change in enthalpy, internal energy, or entropy regardless of the starting value. The difference in thermodynamic reference state amongst the different data sets is unimportant except when the chemicals of the different states interact. The only interaction takes place in the combustion chamber. The NPSS RocketComb1 element already takes the reference state into account via the correction term H_{ref} used when calculating the htMix, the enthalpy of mixture of propellants as they enter the combustion chamber.

$$H_{mix} = (H_f - H_{f,ref})W_f + (H_{ox} - H_{ox,ref})W_{ox} \tag{41}$$

The values for the thermodynamic reference state correction terms are calculated based on the available CEA data. The thermochemical library included with CEA has one data point for each oxygen and methane [20]. The NIST database was then queried

at the same pressure and temperature and the density and enthalpy were recorded. The data can be seen in Table 12.

Table 12: CEA and NIST Propellant Thermodynamic Reference Data.

CEA	BP (K)	P (atm)	Density (g/mL)	Enthalpy (KJ/mol)
CH4	111.643	1	0.4211	-89.233
O2	90.17	1	1.149	-12.979
NIST				
CH4	111.64	1	0.42239	-0.0013586
O2	90.17	1	1.1413	-4.2686

Each H_{ref} can then be calculated for each propellant by taking the difference between the two respective enthalpies and then converting to the NPSS unit of enthalpy, Btu/lb_m.

$$H_{f,ref} = (-0.0013586 - -89.233) = 89.2316414 \frac{KJ}{mol} = 2391.6893 \frac{Btu}{lb_m} \quad (42)$$

$$H_{ox,ref} = (-4.2686 - -12.979) = 8.7104 \frac{KJ}{mol} = 117.0293 \frac{Btu}{lb_m} \quad (43)$$

The values of the reference enthalpy conversions are entered into the respective fuel streams in NPSS in the section for entering initial guesses.

DEAN Changes to Accommodate Methane Fuel

Several updates and changes were made to the DEAN model to achieve a methane based simulation. The starting point of the MDEAN was the sixth iteration of the hydrogen DEAN developed by Simmons. Simmons' work was based on Hall's work, and Hall's work was built on the original DEAN NPSS produced by Martin. Development of the sixth and seventh versions of the hydrogen based DEAN continued in parallel with the development of the MDEAN.

Conical Approximation

As stated in the background section, a large departure from Hall's work is the reliance on conical approximations with regards to the aerospike contour. Hall's DEAN work demonstrated that the conical aerospike developed reasonable approximations for mass calculations while significantly decreasing processing time [8]. Therefore, all nonlinear code was removed from the DEAN code in the transition to the MDEAN.

Pre-Processing

Work by Simmons on the sixth version of DEAN updated the linkage of top level design parameters to underlying model behavior. A major limitation with the existing DEAN was the length of time required for examining the input variable trade space. It was possible and very likely to explore a rocket concept that was not physically realizable. DEAN6 attempts to link internal NPSS geometry inputs into well understood top level geometric parameters, thereby greatly reducing the number of physically meaningless design points. At the same time, this provides the DEAN a clear set of input parameters that can be explored via the ModelCenter parametric study function and the design of experiments function. The input variables are listed in Table 13.

Table 13: Methane DEAN Design Variables.

Design Variable	Unit
Expansion Ratio	N/A
Throat Area	in^2
Chamber Length	in
Characteristic Length	in
Thrust	lb_f
O/F Ratio	N/A

From these input variables, several important geometric values which define a specific rocket design iteration can be calculated. First, used as direct input to the NPSS

rocket, are the chamber and throat outer and inner radii. These four values, combined with Martin's original NPSS assumptions about the shape of an aerospike engine define the contour that combines the combustion chamber to the converging diverging nozzle. The original geometry of the chamber is split up into 6 stations, 5 at the midpoint of equal lengths of the chamber and the final station at the throat. Station five and six are in the converging portion of the design where the outer chamber wall slopes inward. At station six, the chamber wall radius is one inch narrower than the chamber radius at the injection face and station five is half way up the linear contraction at 0.5 inches narrower than the chamber radius at the injection face. A ModelCenter rendered aerospike contour is included in Figure 7 for clarity. Note that this is the initial estimate of conical geometry used to derive relationships required by NPSS. Final geometry uses a more realistic approximation for volume and mass calculations.

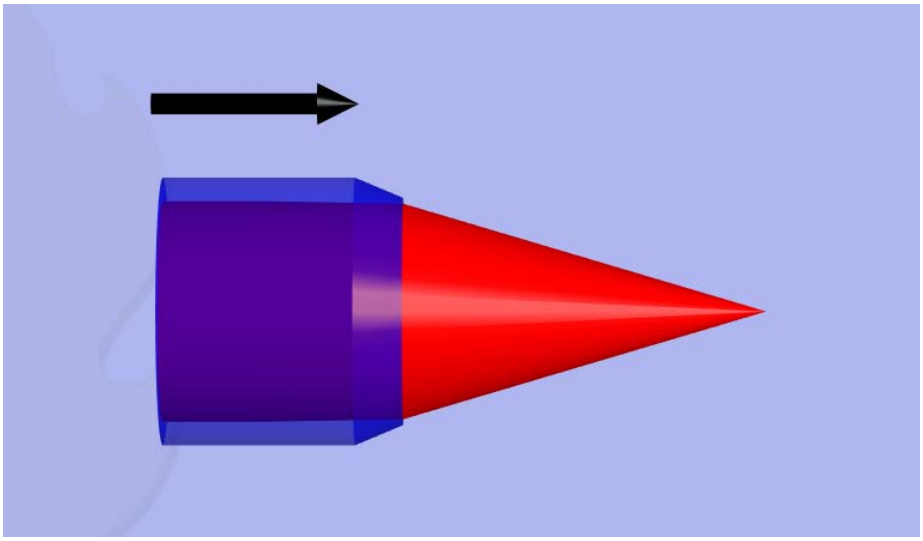

Figure 7: DEAN Conical Aerospike Contour.

In addition to the four radii that define the aerospike, the initial geometric calculations determine the volume of the chamber based on the characteristic length, L^*,

which is equal to the chamber volume divided by the area of the throat. The volume of the chamber is also an input required by NPSS. For a quick check on the feasibility of the input geometry, the injection ratio is calculated as the ratio of the chamber area at the injector face to the area of the throat. For the input geometry to be reasonable, this value must be greater than about two [4]. This limit is based on the areas of the throats that are likely to converge given the requirement of 25,000 lb_f of thrust. This is an imperfect tool as the literature relates the injection ratio to the diameter of a circular throat, but the constraint provides a useful rule of thumb that eliminates the possibility of losing the converging portion of the converging/diverging nozzle. The final geometric calculation to be input into NPSS is the length of the aerospike nozzle. The aerospike nozzle length is approximately the length of a cone nozzle with a half angle of 12 degrees [7].

Initial Input to Cooling Channel Pressure Profiles

When the MDEAN fails to converge, it is usually related to the independent variables and the dependent relationships in the propellant cooling channels. In an attempt to increase the robustness of the model, the initial guesses for the pressure profile through the cooling channels were tied to input parameters. Previous iterations of the DEAN relied on hard numbers coded into the input guesses, presumably captured from converged cases. The method of developing the oxygen pressure profile begins with the input design variables throat area (A_t) and thrust (F). Additionally, a guessed value of I_{sp} is required. For the MDEAN, this guess is 350 seconds. These input values and the rough guess calculate the mass flow rate:

$$\dot{m} = \frac{F}{I_{sp} g_0} \tag{44}$$

With a guess for c^*, the characteristic exhaust velocity, or 6020 ft/s [7], a rough estimate for chamber pressure, P_c, can be calculated with the mass flow rate and the area of the throat, A_t:

$$P_c = \frac{\dot{m}c^*}{A_t} \tag{45}$$

Now the pressure is known at either ends of the propellant feed system. An approximately 5% drop in pressure is assumed from the tanks to the pump inlets. The pressure ratios for all three pumps are input parameters, so the pressure profiles up to the cooling jacket can be estimated. Starting at the other end of the feed system, a 20% pressure loss is assumed for the injector. The pressure drop across the turbine is estimated by taking an average over several converged cases and resulted in a 25% loss for the fuel and a 50% loss for the oxidizer. The oxidizer turbine bypass line was calculated as the average of the entrance and exit of the oxidizer turbine. Therefore, for both propellant feed systems, the pressure profile has been estimated up to the entrance and past the exit of the cooling channels, providing a change in pressure over the cooling channels. This pressure drop is modeled as a constant pressure drop across the stations. These calculations provide an estimate of the pressure profile that is flexibly based on the input parameters and therefore increases the robustness of the model.

NPSS Updates

The specific changes to the NPSS code are outlined in Appendix B. The goals and implications of the updates are discussed in this section.

Thermodynamic Updates

The first major change is the command to utilize the new sources of thermodynamic properties. At the beginning of any NPSS model, if the standard databases will not be used, an alternate must be set with the *SetThermoPackage* command. As discussed previously, the MDEAN uses the fluid property table thermodynamic package. To use the developed tables, the composition of each flow has to be set to match the fluid property table file name and this is usually set as the comp variable within the instantiation of an element. By using the *SetDefaultComposition* command outside an element, any non-specified flow station compositions are set to the specified, default value. The organization of the DEAN NPSS model makes it easy to set the proper compositions. In the DEAN model, methane must be set as the default composition for the methane feed system and must be specified as the fuel inlet composition in the RocketComb1 (the combustion chamber) element. Similarly, oxygen is set at the beginning of the oxygen feed system as the default and is specified at the combustion chamber element oxidizer inlet. The combustion products are set as the default composition before the combustion chamber and are specifically set at the combustion chamber exit.

As discussed earlier, the thermodynamic bases must match amongst the different species/mixtures. This is accomplished through calculations in the combustion chamber element, but the thermodynamic reference states must be specified in the body of the MDEAN code. Both COMB.Fu_I.htRef and COMB.Fl_oxid.htRef are specified in the MDEAN section of code that outlines initial values to start the solver iteration.

Cooling Channel Enthalpy Profile

Both the fuel and oxidizer have guesses for the enthalpy profiles through the respective feed systems. The original values are assumed to be based on converged solutions. The profile for each species was converted to the NIST thermodynamic basis. This was accomplished by starting the calculation update at the pumps, where the thermodynamic state is defined by pressure and temperature. The existing NPSS assumed increases in enthalpy were then applied through the flow system. Several failures of convergence reference the enthalpy of the different cooling channels. Each cooling channel enthalpy is an independent variable which is perturbed in the solver. The methane side enthalpy profile was later replaced by data from a converged run. Future work in the DEAN or MDEAN should include the upgrade of this system to tie these initial enthalpy guesses to model input values. The updated values for pressure and enthalpy lead to a new defined thermodynamic state and therefore the density estimates for the same flow stations were updated.

Pump Changes

In previous DEAN work, the pressure ratios of the fuel pumps were set equal to each other as targets for convergence. This was done by creating a dependent condition in the top level DEAN of the pressure ratio of the first pump is equal to the pressure ratio of the second pump. This usually resulted in a small pressure rise from the first pump, followed by a large pressure rise in the second pump. This was updated in the sixth version of the DEAN so that each fuel pump produced an equal pressure rise. This was accomplished by adding the variable deltaP to the pump element. The dependent

condition in the DEAN was then updated so the variable deltaP was converged over the two fuel pumps. The DEAN now requires the custom element, Pump02.int.

The fuel pump rotational rate in RPM required update based on the fluid properties of the new fuel. The goal for the update was to maintain the specific speed, N_s, of both fuel pumps. The relation uses U.S. customary units as specified [7]:

$$N_s = {21.2N\sqrt{Q_e}}\Big/{(\Delta H_e)^{0.75}} \tag{46}$$

where

N = Actual Pump Speed (RPM)

Q_e = Volumetric flow (ft^3/s)

H_e = Pump Head (ft)

By maintaining specific speed, the same class of pump is preserved; therefore the estimates used for the pump efficiencies can be maintained. The hydrogen pumps operated at a speed of 110,000 RPM and this was updated to 50,000 RPM for the more dense methane based on a different fuel flow rate (the O/F is significantly different), the change in the nature of the fuel pump pressure ratios, and the different fuel density.

Constraints

The DEAN model can converge onto designs that are physically unrealizable. The constraints section of the DEAN attempts to automatically analyze and eliminate converged models that violate a fundamental concept of operation. Currently, the constraints section of code checks for supersonic flow of propellant in the cooling channels and the combustion chamber. Supersonic flow in these regions is inappropriate as it physically unrealizable without a converging diverging nozzle. Sonic flow in these

regions can occur through an expansion of boundary layers. This represents an undesirable design because it involves an inefficient high pressure drop through the flow system and can cause shocks in the flow.

Cooling Channel Mach Number

An important constraint in the development of a mathematically reasonable model that is also physically realizable is the elimination of supersonic fluid velocities anywhere in the design other than the rocket nozzle. The propellant cooling channels constrict to small cross sectional areas to increase heat transfer and accommodate the chamber and nozzle geometry. By simple incompressible flow, the smaller flow area will accelerate the fluid. Additionally, heat is flowing into the fluid from the combustion chamber, increasing the overall energy of the propellant. The highest fluid velocities will therefore be found in the cooling jacket as energy will dissipate from the fluid after the cooling jacket as the two fluids are expanded through the two turbines.

The Mach numbers must stay within limits that would cause shocks in the flow. For oxygen, the Mach number must stay below 0.6. For methane, the Mach number must remain below 0.9 [13]. The sonic velocity for the propellants is a function of fluid state as defined by temperature and pressure in this case. Again, NIST data was available over the range of interest for both fluids. To automate the process of checking whether a run remained within the required boundary, a Kriging interpolation was used to estimate the sonic velocity of the fluid given the temperature and pressure of the fluid station as reported by NPSS. After NPSS has converged, for every fluid station in the cooling jacket, the Mach number is calculated by dividing the fluid velocity by the Kriging estimate of the sonic velocity and if the largest Mach number is greater than the above

limits, an error occurs, warning the user of the violated constraint. Below is a discussion of the validity of the Kriging interpolation.

The oxygen Kriging interpolation has an average error of 2.62% over 201 observations that span the temperature and pressure range of the function. The Kriging design range was developed by observations of NPSS behavior while remembering the ranges recorded by the converged design points developed in past DEAN research. Original estimates were insufficient in range as some iterations of NPSS use very large increases in pressure. The oxygen Kriging was developed using a temperature range of 100 to 1500 Rankin and a pressure range of 15 to 5000 psia. Note the Kriging was developed without any vapor phase data and therefore if the input state of a fluid station is vapor, the Kriging will not deliver an accurate sonic velocity. This is acceptable because the design of the system assumes only liquid and supercritical phases are present in the propellant feed systems. A comparison of NIST data to the Kriging interpolation of the data at the same state as the given NIST data shows the Kriging data is a good fit and is suitable for the automated process (see Figure 8). The data used for the comparison of NIST versus Kriging data from which the average error was derived is a different set of NIST data from which the Kriging interpolation function was derived. Per the Kriging algorithm, the error for the points from which the Kriging interpolation is derived should be zero or near zero [17]. If a selected run point has a maximum Mach number close to the limit of 0.6, the oxygen fluid velocity should be examined against the exact NIST data to verify the validity of the geometric design.

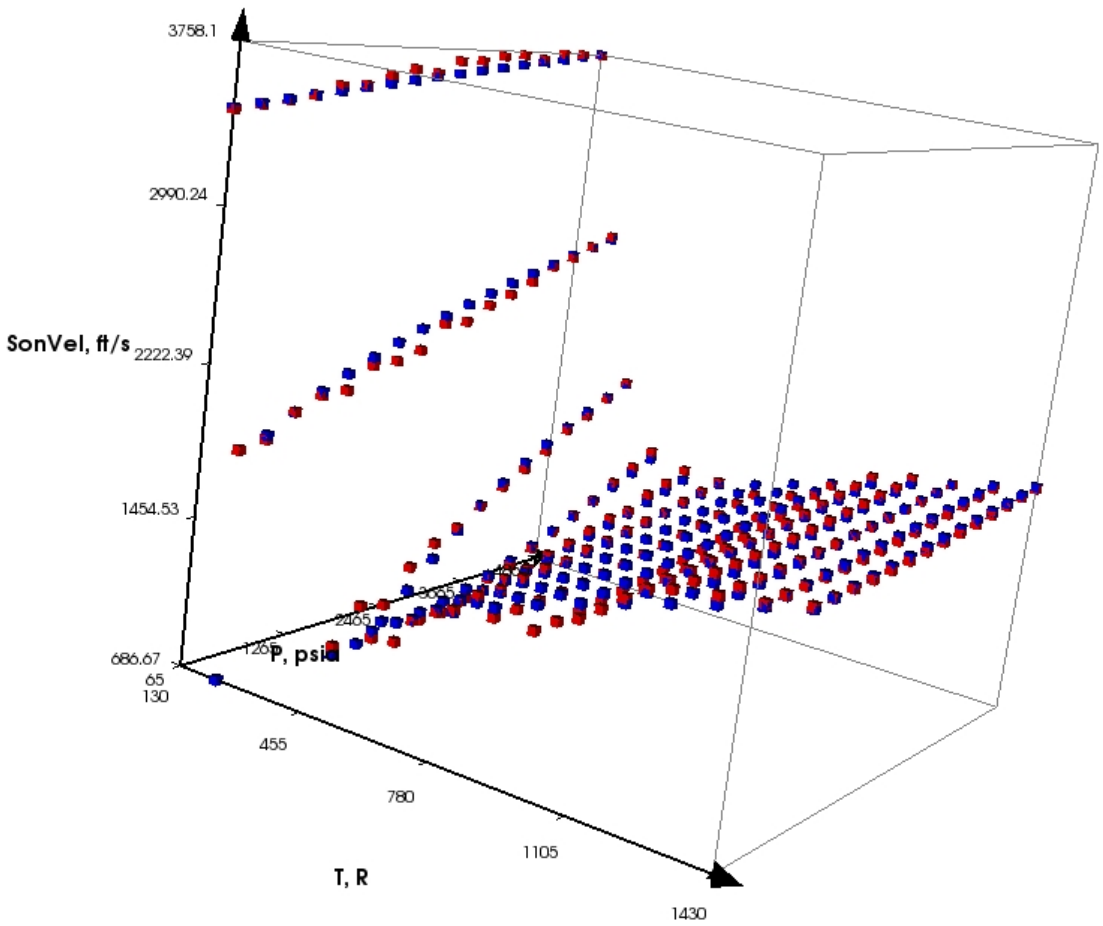

Figure 8: NIST vs. Kriging Sonic Velocity for Oxygen.

Blue = NIST, Red = Kriging Estimate; Sonic Vel = f(T, P)

The fluid velocities at the methane stations are checked in the same manner as the oxygen stations. The methane sonic velocity Kriging interpolation method has an average error of 0.37% over 175 observations across the range of the Kriging. The Kriging was developed over a temperature range of 193 to 1113 Rankin and a pressure range of 100 to 6000 psia. NIST data at high temperatures was limited for methane compared to oxygen, but the available range should be sufficient for the methane feed system. Again, any vapor data fed into the Kriging interpolation will provide

meaningless results. A comparison of NIST source data to Kriging generated data can be found in Figure 9.

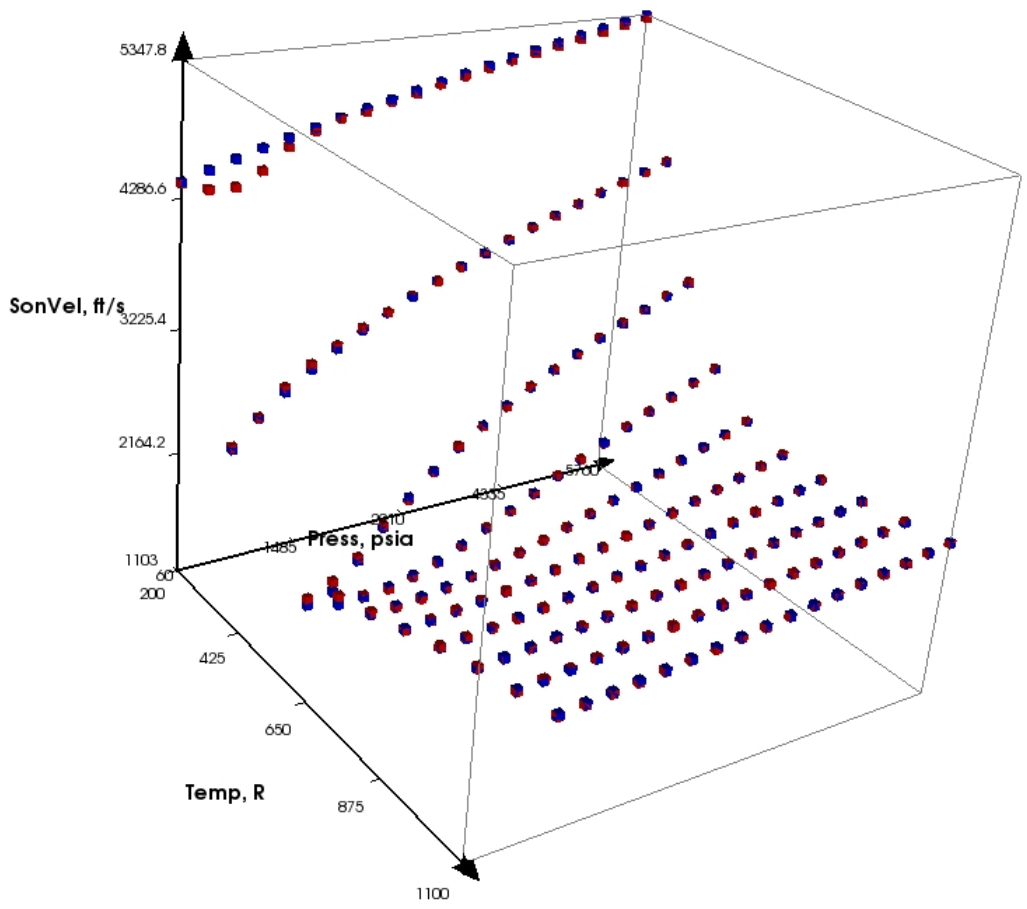

Figure 9: NIST vs. Kriging Sonic Velocity for Methane.
Blue = NIST, Red = Kriging Estimate; Sonic Vel = f(T, P)

Chamber Mach Number

Developed by Simmons for DEAN6, the method for checking the Mach number in the chamber is based on an analysis of the contraction ratio, defined [4]:

$$\frac{A_C}{A_t} = \frac{1}{M}\left[\left(\frac{2}{\gamma+1}\right)\left(1+\frac{\gamma-1}{2}\right)M^2\right]^{\frac{\gamma+1}{2(\gamma-1)}} \quad (47)$$

where

A_c = Chamber's Average Cross-Sectional Area (in^2)

A_t = Area of the Throat (in^2)

M = Mach number in the Combustion Chamber

γ = Isentropic Parameter

The logic in the check subtracts the left side of the equation from the right hand side to find an error term and then iterates the Mach number through a ModelCenter optimization tool until the error term is driven to zero. The resulting combustion chamber Mach number is displayed and should be low to provide time for combustion. The literature suggests the chamber Mach number should be between 0.2 and 0.4 [4].

Post Processing

The post processing calculations were largely inherited from the work of Hall. Additional work to integrate the post processing calculations was undertaken by Simmons in the development of DEAN6.

Angelino Contour

The MDEAN NPSS code calculates energy balances over the system under the assumption of a bell nozzle with an expansion ratio given as an input. This bell nozzle expansion ratio can be equated to an equivalent aerospike nozzle. Hall employed the Angelino method to determine a highly accurate exit Mach number and then a corresponding aerospike nozzle length. This length is then used to develop the spike non-linear contour which unfortunately breaks down for calculating the geometry near

the throat. At this point, Hall used the Angelino length in another program, TDK04, to develop a working contour. Simmons' work in preprocessing first estimates an aerospike length using relations found in the literature [7], a cone using a half angle of 12 degrees. This matches the Angelino approximation well, but for continuity, the Angelino approximation is used for the contour in DEAN6 to avoid the use of TDK04, which is now a superfluous step. Simmons therefore adjusted the Angelino curve to correct for the behavior at the throat. The Angelino contour is then incorporated into the next section of code which calculates the final geometry and mass of the engine. When comparing the Angelino approximation to Hall's work, based on TDK04, the new contour method produced a significantly lower volume and therefore mass. In an effort to maintain a conservative approximation for the thrust to weight ratio, the Angelino contour was averaged with the conical contour that was calculated in the pre-processing steps. The resulting contour matches Hall's more sophisticated contour calculations more closely than the Angelino approximation or the conical approximation. The three different contours can be seen in Figure 10.

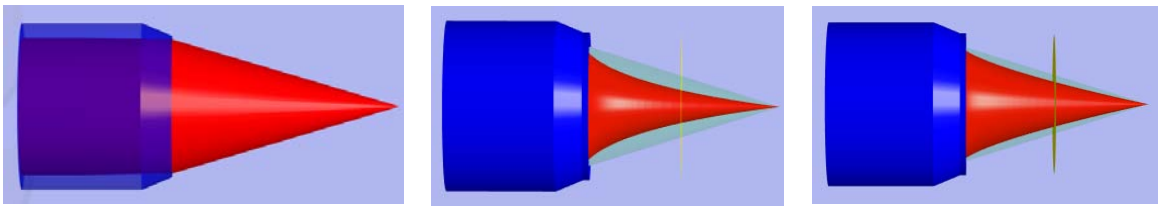

Conical **Angelino** **Averaged**

Figure 10: Three DEAN Estimated Nozzle Contours.

Engine Geometry

Hall's first calculation determines the combustion chamber and nozzle internal geometry along with the maximum temperature of the propellants. These are largely defined through the NPSS code, but the stations need update based on the more detailed aerospike contour. The code assigns the two nozzle stations axial length and radii to the newly calculated non-linear aerospike contour.

These values are then used with material properties of several candidate materials to perform a structural analysis. The structural analysis calculates wall thickness based on the pressures found in the NPSS output. Additionally, material properties are supplied to the ModelCenter calculations as functions of temperature. The software applies curved beam theory to determine if the wall between the propellant channels and the combustion gasses will fail. Based on the NPSS output pressures, the code calculates the bending stress and compares it to the user specified method of failure: yield or ultimate for the designated material. The shear stress is calculated and must be less than the specified material shear strength, which is defined here as one third of the ultimate strength. If failure occurs, the algorithm increases the wall thickness iteratively until the wall withstands rocket operation. The wall thickness data and other previously calculated geometry data are then sent to the next script for mass estimation.

Thrust to Weight Calculation

The final DEAN performance calculation was developed by Hall and integrated into DEAN6 by Simmons. The script calculates the volumes and masses of the chamber, aerospike, plumbing and the mass of the turbo-machinery. The chamber and aerospike are broken up into structural components and cooling channel components. The

geometry is defined in the previous ModelCenter scripts to feed the volume calculations in this script. With component volumes and material densities, the mass of the different components are calculated. Additionally, the turbopump masses are calculated from the following engineering correlation [4].

$$m_{tp} = A\tau^{B} \tag{48}$$

where

m_{tp} = mass of the turbopump (kg)

A = empirical coefficient (1.5 for development)

τ = pump shaft torque (Nm)

B = empirical exponent (0.6 for development)

Plumbing length and therefore mass is estimated at twice the engine length (nozzle length plus chamber length) while the hardware mass is estimated as five percent of the total engine mass. The percent hardware is treated as a design variable and can be adjusted as necessary. Five percent was chosen for consistency over the different DEAN projects. All of the mass is then summed to find a total engine mass. With the NPSS calculated thrust, the figure of performance, thrust to weight, can be calculated.

The key task in the exploration of the MDEAN is the development of fluid property tables that accurately provide thermodynamic values for a defined state. The propellant tables were built using online NIST data and the combustion products tables were built using the chemical property estimation program CEA. The tables were then integrated to the concurrently developed DEAN6 model through several changes to the different model components. After some debugging and validation, the MDEAN model

was exercised over a wide range of the input design variables. The results of these runs are discussed in the following chapter.

IV. Analysis and Results

This chapter will discuss the results of the MDEAN research. First, the error associated with the new fluid property tables is explored. Then the results of the runs of the MDEAN model are examined to find interesting performance estimates over a wide range of the design variables. A variety of thrust levels were explored, and one of the more promising design points at 25,000 lb_f of thrust is selected for a more in depth analysis to determine if the rocket is physically realizable. Finally, the chosen rocket concept is compared to several other rockets.

Oxygen FPT Error Analysis

The oxygen fluid property tables were more complex in construction than the methane fluid property tables, but were similar in concept in that the source NIST data must be reorganized from being defined by the independent variables of pressure and temperature into data tables that define the state of the fluid by enthalpy and pressure. Several different methods of data manipulation were required to obtain sufficient accuracy in property values. First, a Kriging fit was initially used over the entire range of required data to include liquids and supercritical fluids. Error for this interpolation was such that the resulting tables were deemed insufficient. The data sets input to the Kriging interpolation algorithm generation were therefore split by phase. The data boundaries for the two Kriging interpolators are found in Table 14.

Table 14. Independent Variable Ranges for Oxygen Fluid Property Tables.

Phase	P_{Low} (psia)	P_{High} (psia)	H_{Low} (Btu/lb_m)	H_{High} (Btu/lb_m)
Liquid	15	4000	-74	-11
Super Critical	750	4000	-5	220

The quality of the interpolation algorithm is determined by simple comparison of R^2 values of the models, to determine a qualitative, but relative comparison of the quality of the estimation. The R^2 for the C_p Kriging function over the entire data set was 72.44%, insufficient for the purpose of tabulating values. By splitting the data sets by phase, the liquid phase R^2 was 99.925%, but the super critical R^2 was still too low for use. To increase accuracy of the oxygen C_p and ratio of specific heats (γ) thermodynamic properties in the super critical phase (which will be encountered in the cooling channels), the following definitions of the properties were used.

$$C_p = \left(\frac{\partial H}{\partial T}\right)_P \tag{49}$$

$$\gamma = {}^{C_P}/_{C_V} \tag{50}$$

These definitions were employed in two different ways. The γ parameter is simply solved for in the NPSS interpolation tables by replacing the table with a function that calls for the corresponding C_p and C_v values, which are tabulated. C_p is estimated through a numerical approximation of the partial derivative of enthalpy with respect to temperature at constant pressure. Temperature, pressure, and enthalpy data was generated via the super critical Kriging interpolator. A sufficient range of enthalpy and pressure data was input, and the temperature was estimated as an output. This data was placed in a spreadsheet and sorted by pressure and then the following numerical derivative was applied to estimate the constant pressure specific heat.

$$C_p|_x = \left(\frac{H_{x+1} - H_{x-1}}{T_{x+1} - T_{x-1}}\right) \quad (51)$$

At the edges of the blocks of constant pressure data, C_p values were taken directly from the NIST database. Additionally, data was spot checked against the NIST database and it was found that data near the critical point (T=278 R, P=731 psia) had significant error. Data in this region was replaced with NIST data.

The fluid property tables were then tested for accuracy against the NIST database. The Kriging estimator directly supplies the values that were used in its generation when queried for an observation at such a point; therefore a new set of data was generated to test the interpolation. The data from the Kriging was generated over the range of data that was used for generation. The results of a comparison to NIST data can be found in Table 15. The n column is the sample size and each other number is the percent error.

Table 15: Kriging Interpolation Percent Error As Compared to NIST - Oxygen.

Data	**n**	**H**	**Density**	**K**	**C_v**	**C_p**
Liquid	38	0.28	0.03	0.05	0.07	0.17
Sup Crit	61	2.48	1.95	0.81	0.58	1.55
Combined	99	1.64	1.21	0.52	0.39	1.02
Data	**n**	**Visc**	**U**	**S**	**Gamma**	
Liquid	38	1.17	0.05	0.13	0.22	
Sup Crit	61	2.34	2.18	0.15	2.47	
Combined	99	1.89	1.36	0.14	1.61	

The average errors for the thermodynamic properties are reasonable when averaged across the range of states that are of interest to the rocket problem. Error still spikes near the critical point as demonstrated by Figure 11.

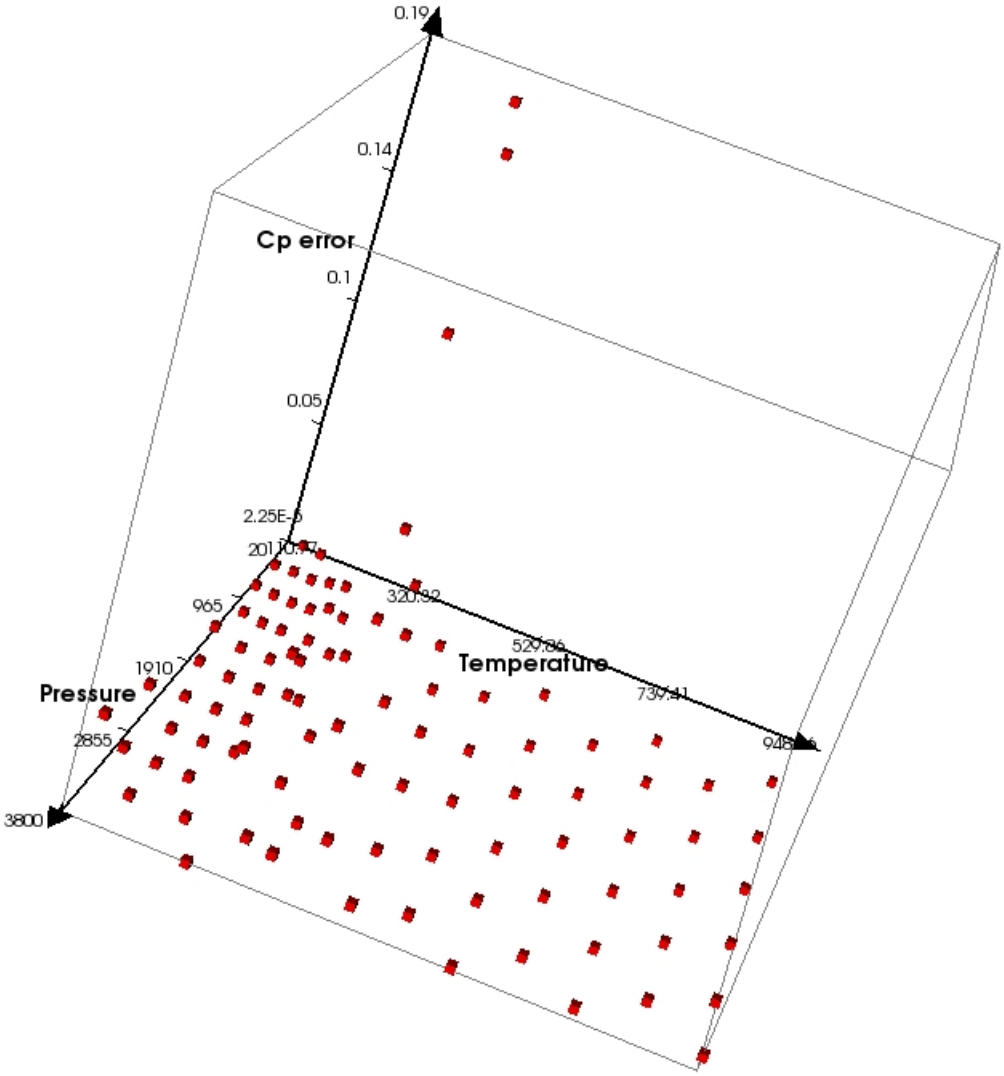

Figure 11: Kriging Oxygen C_p Error as a function of Temperature and Pressure.

Figure 11 depicts a spike in error of approximately 20% in the region of the critical point (T = 278 R, P = 731 psia). Based on the method of data collection for the error analysis for the super critical region, this is a high end estimate of error. The data included in the NPSS interpolation tables for this region is directly from NIST and therefore any error associated with it will be from linear interpolation between two points. For this region in the error analysis, the closest tabulated value was used, and therefore it would be expected error would be less for a linear interpolation. The

approximately 20% error in this region is therefore a high end estimate over a relatively small region.

Methane FPT Error Analysis

Error associated with the methane fluid property tables is significant, but was controlled through the iterative improvement of the methods of estimation. As discussed previously, the source NIST data is organized by temperature and pressure while NPSS data must be organized primarily by enthalpy and pressure. A Kriging estimator controlled through ModelCenter reorganized the data via Kriging regression and created the necessary tables, and NPSS then utilized the tables for property estimates through linear interpolation. The two different interpolation methods have different methods of reducing error. The Kriging works best when the data is spread evenly over the area of interest with enough fidelity (small step size) to capture non-linear behavior, but if the sample size is too large (over 1000 points), the tool will break down. On the other hand, a small step size with data concentrated in the areas of interest will reduce error for the linear interpolation.

The first attempt of table generation was a failure because the span of data was too large. The problem was then broken down by phase so that two Kriging estimators could better estimate over the range of interest. Upon examination of the input data, it was noticed the low end of the temperature/enthalpy range was neglected with regards to data count. This was remedied with the additional more NIST data. The rebuilt Kriging estimators improved to a useful point. The errors associated with the Kriging estimators are in Table 16.

Table 16: Kriging Interpolation Percent Error As Compared to NIST - Methane.

n	H	Density	K	C_v	Visc	U	S	Gamma	C_p
153	9.65%	1.33%	1.20%	0.26%	2.27%	4.61%	11.15%	2.98%	3.02%

Although the error for enthalpy and entropy is significant, in the interest of time and because the error is concentrated in one location, it was decided to discontinue the effort of reducing the estimation error. This decision was made because the primary source of estimation error remains at approximately 20% in the estimation of the heat transfer coefficients via the Bartz empirical relationship. Additionally, the error consistently occurs at low temperatures (200 Rankin and below). The only place this state exists in the model is before the fuel pumps. Because the cooling volume element, CoolingVolume02.int, uses enthalpy and pressure to define the state, the error at this location could propagate to the other fluid properties. It is therefore recommended that the low temperature methane error associated with the Kriging estimator be reduced further before additional research is undertaken with the methane fluid property table files.

To demonstrate that the calculation error for enthalpy is located at the lower temperatures, the error calculation is repeated on the same data set after eliminating data below 200 Rankin. This can be seen in Table 17.

Table 17: Kriging Interpolation % Error Compared to NIST, Methane: > 200R.

n	H	Density	K	C_v	Visc	U	S	Gamma	C_p
137	1.03%	1.44%	1.23%	0.24%	1.96%	3.12%	10.27%	3.26%	3.36%

It is unreasonable to ignore this error because the fuel feed system does have a section that is at a low temperature and at least one element in this region uses the

enthalpy to define the state of the fluid. The large entropy error is not a concern for the MDEAN as none of the MDEAN elements employed entropy to define the state.

Combustion Products FPT Error Analysis

The first several iterations of the combustion products fluid property tables were unsatisfactory with regards to error. The error in this table came from two different sources, the NPSS linear interpolation and the method of generation of the reverse lookup table, temperature as a function of enthalpy, pressure, and O/F ratio, T=f(H,P,O/F). Initial iterations had significant linear interpolation error due to poor choices in step sizes for the independent variables in the regions of interest. Of the few initial points of NPSS convergence, the area of interest for this table is defined as pressure from 1600 to 1700 psia and a temperature of 6000 to 7000 Rankin. Nonlinear behavior is detrimental to the linear interpolation process, but it can be minimized through decreasing step sizes in important regions.

Initial guesses of step sizes in the area of interest sometimes caused linear interpolation error on the order of 36% (at a single point in the area of interest). The method of reducing this error was to add significantly more data in the region. Increasing the number of data points from 2500 to 5500 reduced interpolation error considerably. The average error across the all of the thermodynamic properties in the area of interest is negligible as described in Table 18.

Table 18: Average Error in Area of Interest by Thermodynamic Property.

Property	Average Error	N
Enthalpy	0.00012%	33
Density	0.00005%	33
Gamma	0.00000%	33
C_p	0.000075%	33
Thermal Conductivity	0.00005%	33
Viscosity	0.00015%	33
Entropy	0.000009%	33
Internal Energy	0.00046%	33

There is error associated with gamma, but it is on the order of rounding error and therefore was not seen in the error calculation. The percent error was calculated by comparing the NPSS output value of the thermodynamic property to the CEA calculated value. The NPSS output values were obtained by exercising the solver over one iteration and observing the properties assigned to the exit port of the RocketComb1 Element. O/F was held constant at 3 for the purpose of this measurement. The CEA comparison data was developed by using the ModelCenter carpet plot function on a quick-wrapped CEA. Further error analysis would improve confidence, but because of the small error associated with the linear interpolation, further error analysis on this table will not be undertaken. Additionally, the method by which the data was generated, through CEA, and that the table values are considered true (as compared to the double interpolated values of the reactant's tables) suggests that this portion of the combustion products table is of comparably high quality.

Another source of error with respect to the combustion products thermodynamic properties is the reverse lookup table, temperature as a function of enthalpy, pressure, and O/F. This table is notably employed in the combustion chamber to set the state of the flow at the injector face. This state and the combustion chamber exit port state are used

to calculate the energy balance across the combustion chamber, which is an important dependent relationship for the MDEAN convergence. The error associated with this table was originally due to two interpolations, first a Kriging to build the table and then a linear interpolation. The error was significant and challenging to measure and ranged from an average of 10% to an average of 35% over the various experiments that utilized this method. A different approach was attempted that eliminated both sources of error and introduced another that was easily quantified. The fluid property tables can use functions instead of tables and this method was used in previous tables with only two independent variables. The three dimensional function was developed using a stepwise, cubic regression in ModelCenter. The increase in data density for the combustion products tables discussed above provided enough data to create a polynomial with suitable accuracy over the range of possible enthalpies, pressures, and OF ratios. The adjusted R^2 for the polynomial is 96.08%. Although this is not a great fit when compared to the Kriging fits for the propellants, further analysis suggests that it is sufficient for this effort.

The error associated with the polynomial is easy to calculate using a spreadsheet and the original data used for the polynomial generation. The average error associated with the polynomial over the span of data used for generation is 2.98%, examined over 5500 data points. Of the 530 data points that were within the area of interest, the average error is 1.22%. **Error! Reference source not found.**There is significant error when using this polynomial model. However, most of the high values of error are found at the extremities of the problem, at very low pressures or very low enthalpy. These conditions are not usually associated with combustion chambers. In the region of interest, there is still error associated with the polynomial approximation of temperature, but the

maximum error is about 4% and is associated with an O/F ratio of 4.25. Based on earlier discussion of the optimal O/F ratio given an expansion ratio, it is unlikely the MDEAN will have optimal performance beyond an O/F of four.

Another solution to calculate the temperature exists and initial tests show that it is compatible with NPSS fluid property table syntax. It can be inferred from observing **Error! Reference source not found.** that a better fit could be obtained for the data by running cubic regressions over data sets of constant OF. Each OF ratio has a different error curve, suggesting different polynomials will fit the different curve better than a unified polynomial. Polynomial development supports this assumption by examination of adjusted R2 values which can be found in Table 19.

Table 19: Adjusted R^2 for Constant OF, T = f (H, P) Polynomials.

OF Ratio	Adjusted R^2	# Data Points
2	96.65	1250
3	95.71	1250
3.5	95.56	1250
4	96.27	1250
5	95.96	1250

These models obtained similar levels of successful fit with roughly 20% of the data used in the variable O/F polynomial. With additional data and additional logic in the fluid property table function, an increase in accuracy might be realizable. The logic in the fluid property table is complex as the tables do not support simple if, then, else logic operators. There is a workaround with a C/C++ computational equivalent, the ternary operator, '?'. In addition to calling the proper functions, this method would also require an interpolation to use O/F ratios other than those supplied as polynomials. Because of the added complexity of writing the logic to include interpolation, the more straight forward solution, a three dimensional polynomial, is employed.

Run Point Generation – 25,000 lb_f

The model design space was developed over the five variables expansion ratio, throat area, chamber length, characteristic length, and oxidizer to fuel ratio. The first exploration maintained the thrust variable at 25,000 lb_f, and it included 2274 runs of which 541 converged (23.8%). The thrust level was chosen to accommodate the NGE goals outlined previously. The first exploration was over the five listed design variables and included the search outlined in Table 20.

Table 20: Initial Search. 25,000 lb_f Thrust.

Design Variable	Low Value	High Value
Expansion Ratio	4	40
Throat Area (in^2)	8	20
Chamber Length (in)	8	32
Characteristic Length (in)	40	61
O/F Ratio	2.2	4.9
Number of Levels	4	

Subsequent runs expanded on areas of convergence and extended the expansion ratio to 60. The goal of the high expansion ratio runs was to find designs that met the goal for I_{sp}. In the high expansion ratio exploration, the rate of convergence dropped to approximately 13%. The two figures of merit calculated by the model are specific impulse and the thrust to weight ratio. Figure 12 shows the results of the 541 converged cases plotted as I_{sp} against thrust-to-weight. The vertical line represents the NGE thrust-to-weight goal of 108 and the horizontal limit for I_{sp}, the top of the graph, is 383 seconds because no points met or exceeded the NGE goal.

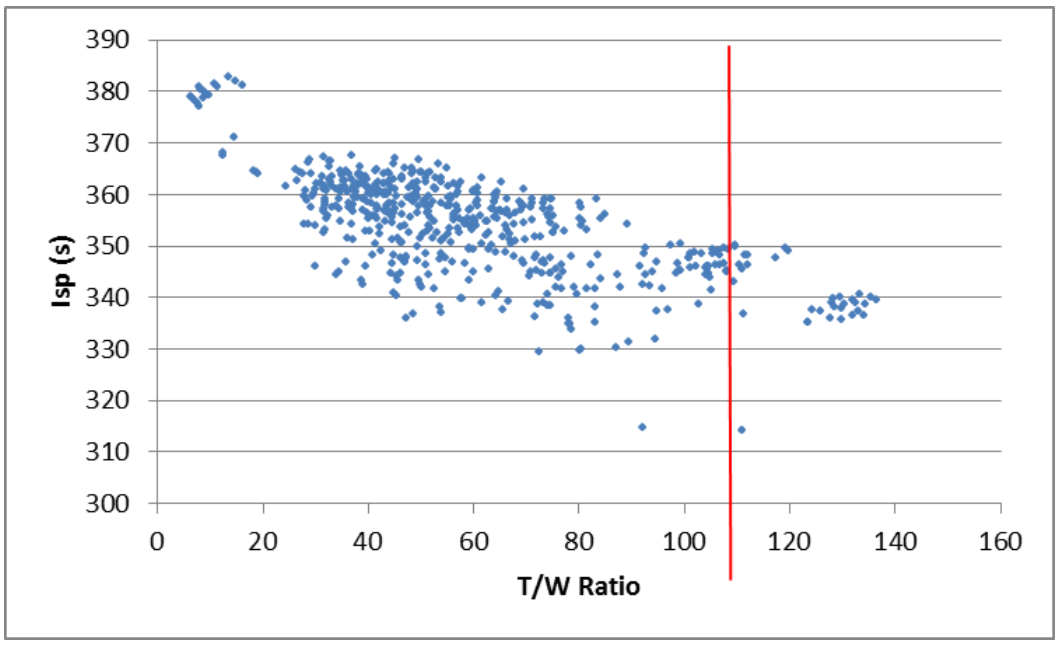

Figure 12: I_{sp} Versus Thrust-to-Weight. 25,000 lb_f of Thrust.

Because no points reach the goal of 383 seconds of I_{sp}, a point with thrust to weight ratio greater than 108 was initially selected for further analysis. The process for selection was based on the concept of a Pareto frontier, which is described as the subset of values which are Pareto efficient. A Pareto efficient point is one where there is no opportunity for a Pareto improvement. A Pareto improvement is a change from one point to another where there is an improvement in one value without a corresponding reduction in the other value. The area of the above Figure 12 where thrust-to-weight is greater than 108 is expanded in Figure 13. The Pareto efficient points are circled and can be grouped into two basic groups based on I_{sp} where the 3 points on the left are at about 350 seconds and the 3 points on the right are at about 340 seconds. The point with the highest thrust-to-weight from the grouping of the higher I_{sp} values was selected for further exploration in the following section.

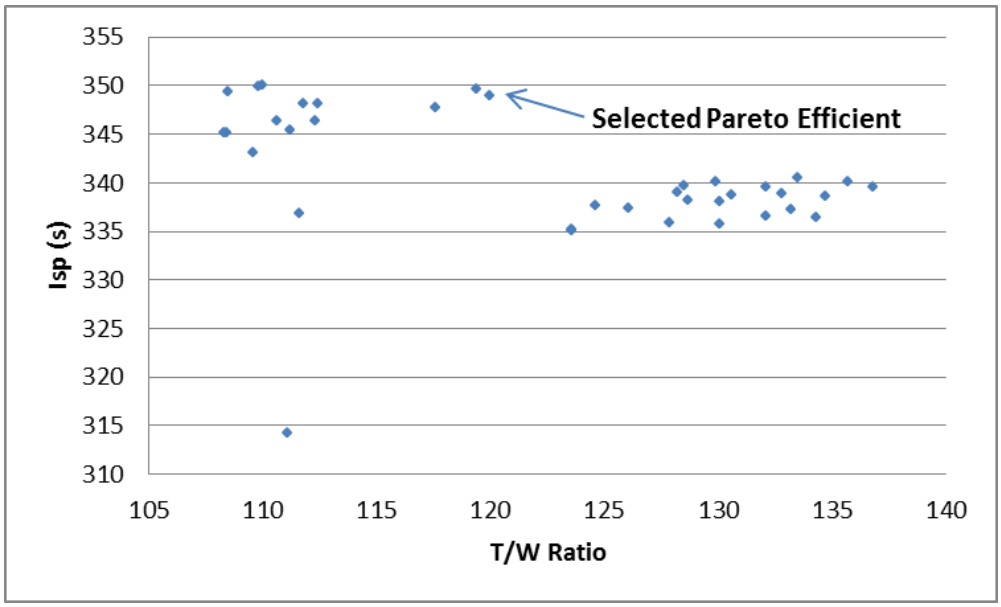

Figure 13: High Thrust to Weight Ratio Pareto Front at 25,000 lb_f Thrust.

The first point to be analyzed further is described in Table 21. The initial point is from the data set above, marked on Figure 13, and the second point is the result of parametric sweeps over each input design variable. The goal of these parametric sweeps was a crude attempt at optimization. ModelCenter supports a more thorough optimization package, but it was not employed due to time constraints and fragility of the MDEAN model. The design point after the parametric sweeps serves as the engine concept selected for further developed.

Table 21: Design Point of Interest.

	Initial Point	After Parametric Sweeps
Expansion Ratio	7	7
Throat Area (in^2)	8.5	8.4
Chamber Length (in)	11	11
Characteristic Length (in)	50	50
O/F Ratio	3.3	3.25
Specific Impulse (s)	349	349.3
Thrust to Weight Ratio	120	120.7

Alternate Engine Concepts

Because of the automation capabilities of ModelCenter, the MDEAN search expanded into other interesting ranges of exploration. As discussed above, the first exploration away from the areas of likely convergence was high expansion ratios. The operational upper stage engines with large values of I_{sp} utilize bell nozzles with very large expansion ratios. For an aerospike, a large expansion ratio is directly related to the size of the engine. It is expected that a higher expansion ratio (needed to achieve a higher I_{sp}) is defined as a larger engine and would in turn have a reduced thrust-to-weight. Table 22 describes one point that reached the I_{sp} goal after some additional exploration with parametric sweeps.

Table 22: High I_{sp} Design Point of Interest at 25k lb_f thrust.

	Initial Point	After Parametric Sweeps
Expansion Ratio	60	60
Throat Area (in^2)	8	8
Chamber Length (in)	14	14
Characteristic Length (in)	50	48
OF Ratio	2.75	2.75
Specific Impulse (s)	382.9	383
Thrust to Weight Ratio	13.8	14.3

This point will not be explored in detail because of the poor thrust-to-weight ratio. It is an interesting data point because it is representative of the magnitude of tradeoff it would take to achieve the derived NGE I_{sp} goal. The relationship between mass, expansion ratio, and I_{sp} is explored in Figure 14. This plot was generated by a parametric sweep over expansion ratio keeping all other design variables constant. The static design variables are outlined in Table 23.

Table 23: Additional Design Variables for Expansion Ratio Sweep in Figure 14.

Throat Area (in^2)	9
Chamber Length (in)	12
Characteristic Length (in)	50
Oxidizer to Fuel Ratio	3

The I_{sp} performance of the rocket increases asymptotically to a level near the goal of 383 seconds. At the same time, the engine mass increases almost linearly so there are diminishing returns to increasing the expansion ratio on the MDEAN.

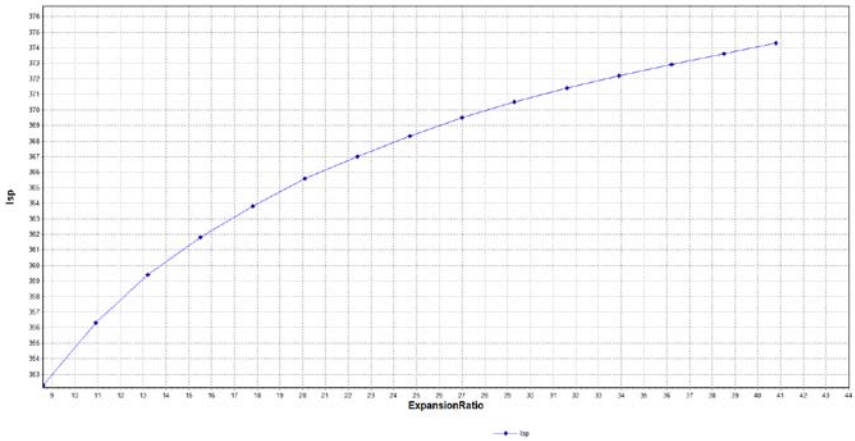

(a) I_{sp} vs. Expansion Ratio

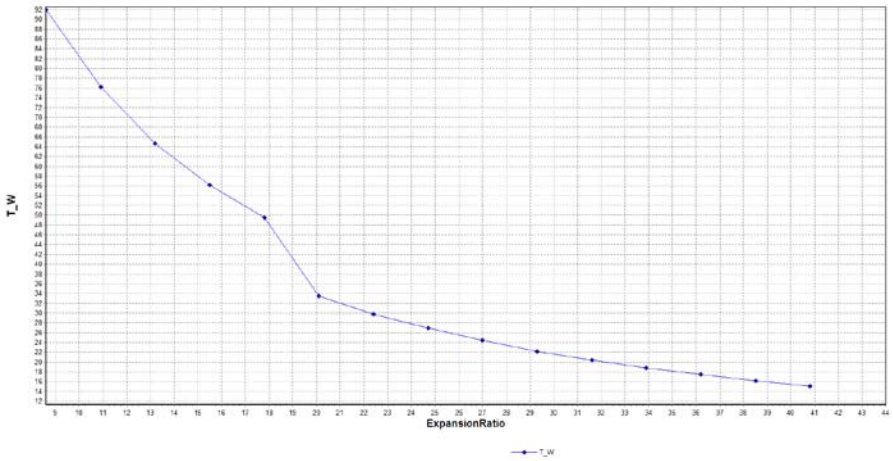

(b) T/W vs. Expansion Ratio

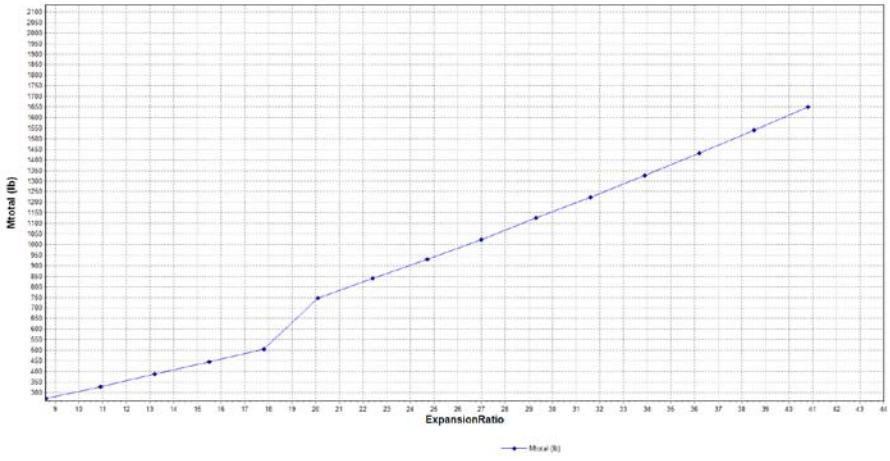

(c) Engine Mass vs. Expansion Ratio

Figure 14: Effect of Expansion Ratio on I_{sp}, T/W, and M_{engine}.

Alternate levels of thrust were explored in an effort to find interesting performance estimates. First, thrusts of 10k, 15k, and 20k lb_f were explored and the results are graphed as I_{sp} versus thrust-to-weight in Figure 15. None of the explored, converged points met the goal for I_{sp} and only one point approached the goal for thrust-to-weight. The low thrust options were explored for the possibility of combining multiple engines.

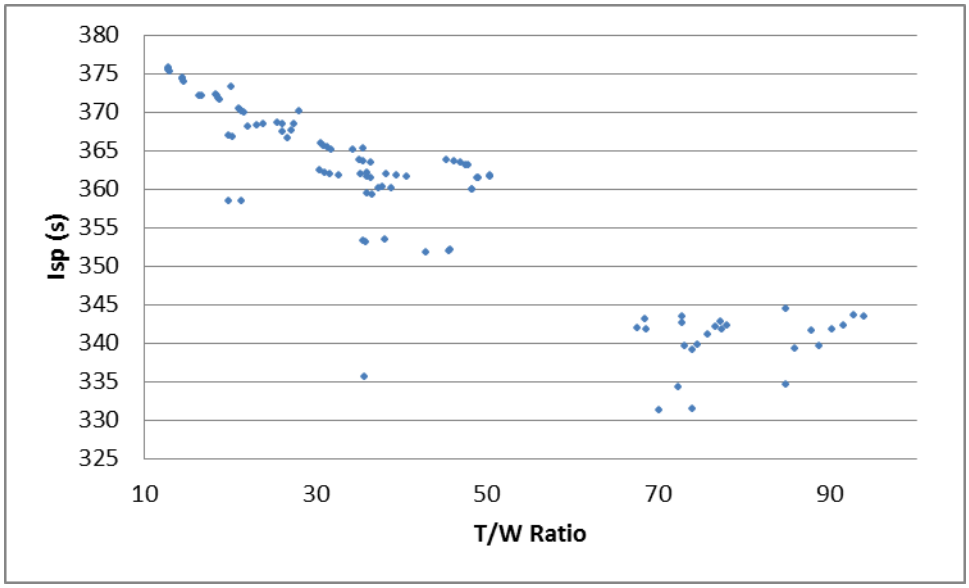

Figure 15: I_{sp} Versus Thrust-to-Weight. Thrust = 10k, 15k, and 20k lb_f.

Next, the thrust levels were increased to 30,000 pounds of thrust and the performance results can be seen in Figure 16. Again, performance is similar to that found at 25,000 pounds of thrust.

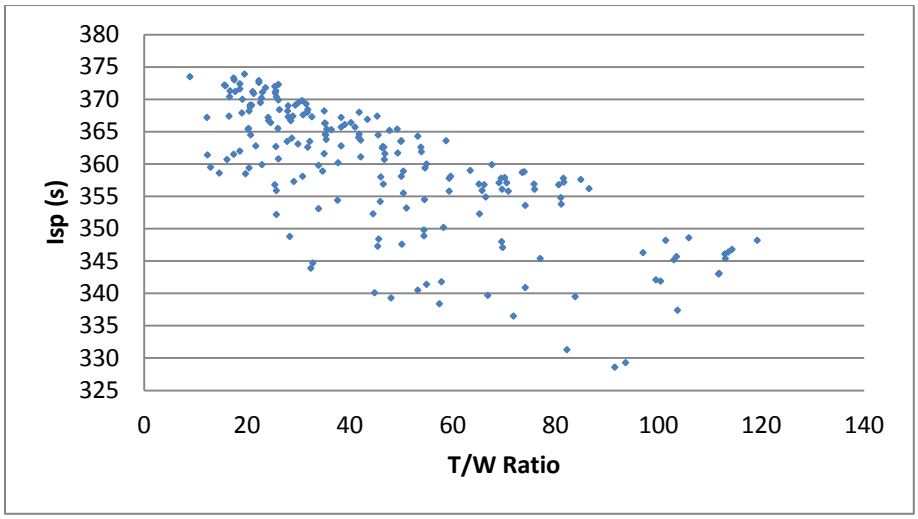

Figure 16: I_{sp} Versus Thrust-to-Weight. Thrust = 30,000 lb_f.

Figure 17 shows the performance of the converged MDEAN designs at 35,000 pounds of thrust. This scan was over 1296 runs with 75 design points converged (5.8%). This thrust level provides no points that are more interesting than the 25,000 lb_f of thrust exploration. The lower rate of convergence suggests the cycle balances less often.

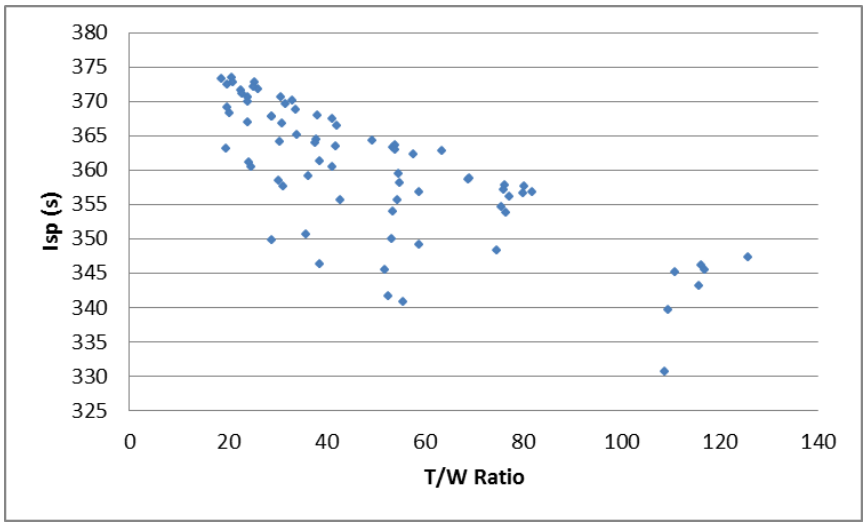

Figure 17: I_{sp} Versus Thrust-to-Weight. Thrust = 35,000 lb_f.

Exploration of Selected Run Point

Several physical constraints are checked throughout the model in an effort to eliminate run points which represents physically unrealizable designs. This section discusses those considerations and explores the feasibility of the chosen input parameters.

The checks related to the combustion chamber are related to the gas flow velocity in the combustion zone and the injection ratio. The Chamber Mach number is 0.13. This satisfies the requirement that the chamber fluid velocity be "slow." The injection ratio is the chamber flow area at the injector divided by the area at the throat and should be greater than about 2 as a rule of thumb. The Injection Ratio is 5.05.

The cooling jackets are critical to the convergence of the NPSS simulation as they provide the energy flow for the dual expander cycle. The first of the constraints concerning the two cooling jackets is the fluid flow must not approach or surpass sonic velocity. The maximum fuel Mach number is 0.09283 and the maximum oxidizer Mach number is 0.15837. These seem acceptable if not a bit slow. The coolant velocity in the cooling channels is related to the rate of heat flow across the wall. This suggests there is plenty of margin to reduce the depth of the channels to increase the velocity of the fluids. If the wall temperatures of the cooling jackets are too hot, it would be important to increase the fluid velocity. The wall temperature profile is shown in Figure 18. The breakdown point of silicon carbide is 5405 Rankin and it is shown as the horizontal line on Figure 18. The X axis on Figure 18 is axial distance from the injector face in inches with the throat at 11 inches. The two final stations on the spike side cooling jacket are on the aerospike, outside of the engine. The maximum temperature is on the spike side at a temperature of 3531 Rankin. This is a significantly higher wall temperature than was

experienced in Hall's DEAN model, about 1000 Rankin [4]. One advantage of the cryogenic hydrogen is its excellent coolant qualities. This difference in cooling effectiveness necessitated a change in the spike cooling jacket material from oxygen free copper to silicon carbide. Silicon carbide has favorable properties at high temperatures but creates challenges in manufacturing.

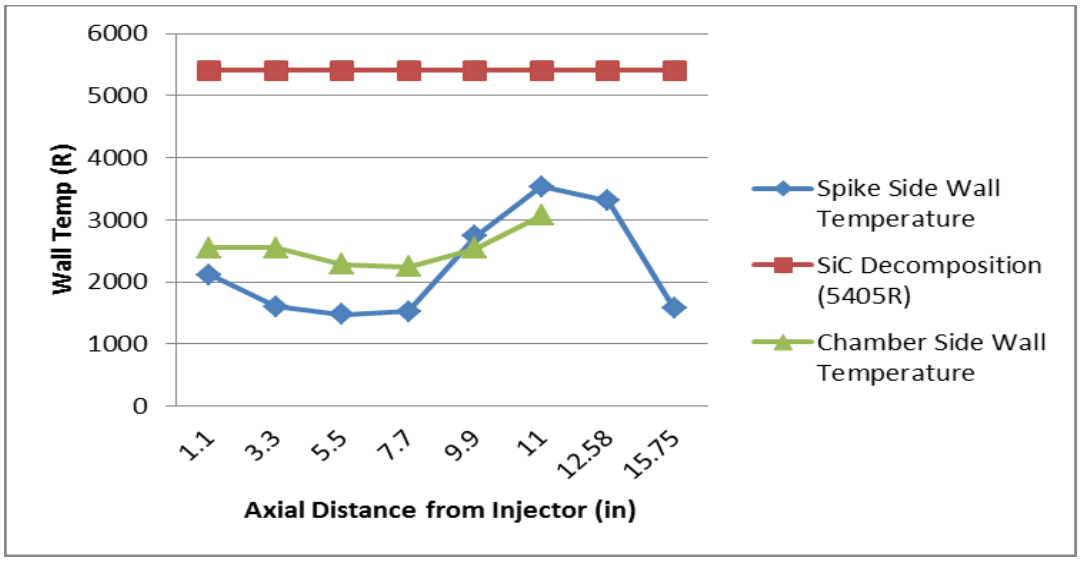

Figure 18: Wall Temperature Profiles for Cooling Jackets.

In addition to the temperature profile, the pressure profile is important to the proper function of the cooling cycle. Figure 19 shows the pressure drops across the two cooling systems. The curves seem reasonable and the fuel pumps increase the fuel pressure by equal amounts, as expected in this version of the MDEAN.

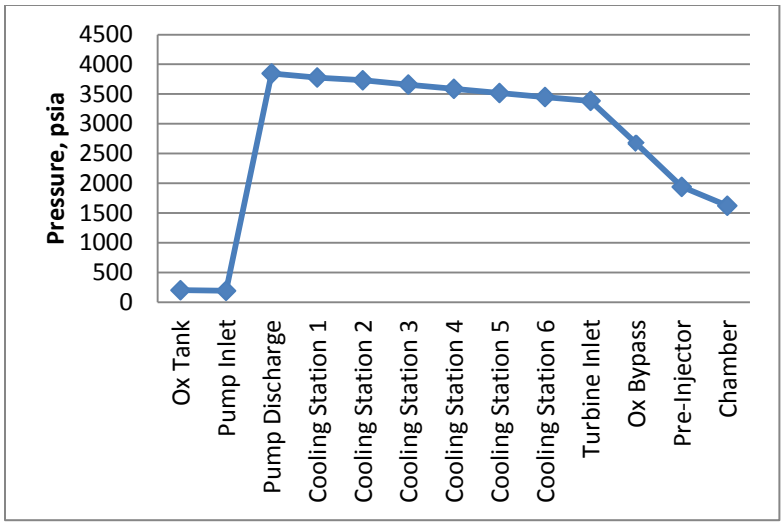

(a) Oxidizer

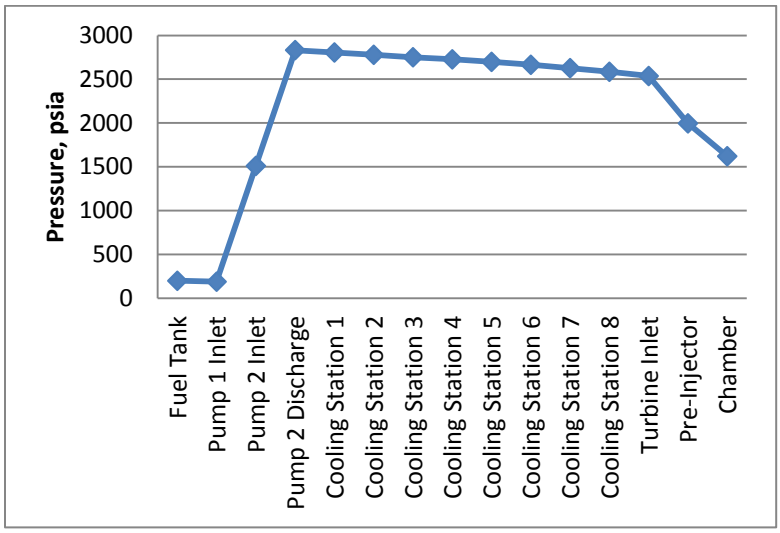

(b) Fuel

Figure 19: Propellant Feed System Pressure Profile.

An important constraint on the pressure profile is the injector pressure drop which should be approximately 20% to 50% of the chamber pressure. The oxidizer pressure drop across the injector is 317 psia, or 19.56% of chamber pressure. The fuel pressure drop across the injector is 375 psia, or 23% of chamber pressure. Although the oxidizer side is a bit low, this was deemed acceptable. It would be ideal to increase the pressure of the fluid before the injector. As it stands, there is insufficient margin to increase the

fluid velocity through the oxidizer cooling jacket. Although the wall temperature could be reduced, the pressure drop through the cooling jacket would increase, reducing the pressure at the injector.

The final check is against the aerospike thickness. The walls of the aerospike are built up by three layers. The cooling jacket is the interface with the combustion side hot gases. Below the cooling jacket are the cooling channels of defined thickness and depth. Supporting these is a structural jacket. The remainder of the radius (near the center of the spike) is hollow. The thickness of each component and the radius of the spike at every station are all independently calculated. For every station, the three layers of the spike are checked against the radius of the spike. If the sum of the layers is greater than the spike, the MDEAN rejects the run point.

The physical dimensions of the MDEAN are displayed in Figure 20. The small physical size of the DEAN family of rockets is an important characteristic.

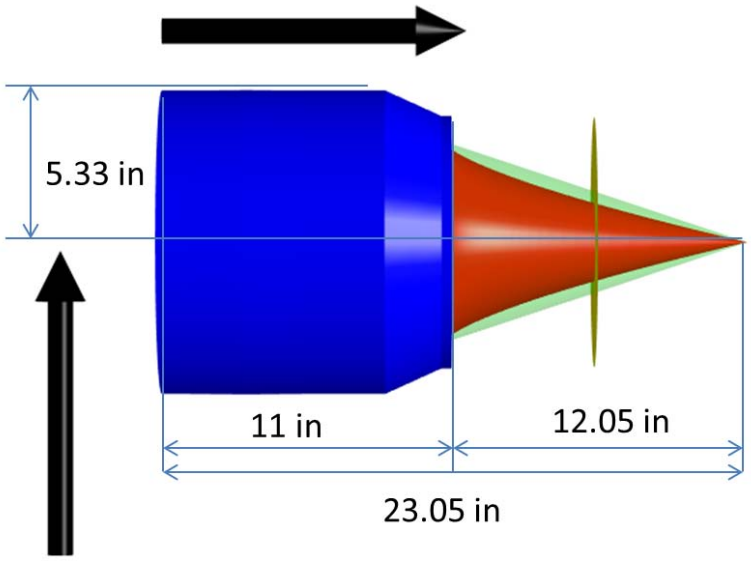

Figure 20: The MDEAN Physical Dimensions.

The MDEAN volume is well under the NGE spatial requirements of 90 inches from gimbal to nozzle exit and an exit diameter of 73 inches [5]. For those missions that have challenging volume requirements, the MDEAN's comparatively small size might be beneficial. A scale comparison of the NGE requirements to the selected MDEAN engine is shown in Figure 21. Additional length savings can be realized through truncation of the aerospike with a small loss of performance [8, 13].

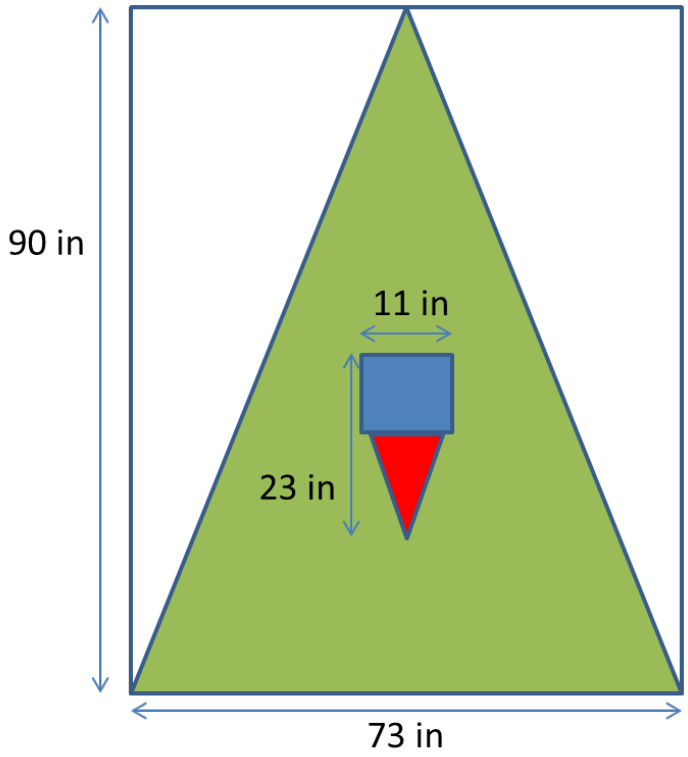

Figure 21: MDEAN Overlaying the NGE Spatial Requirements.

Comparison of MDEAN

In this section, the MDEAN is compared to several other rocket concepts. Table 24 shows the primary performance parameters for several different rockets, now including the MDEAN.

Table 24: Comparable Engine Performance.

Engine	MDEAN	RD-185	RD-167	RD-160	NGE_{Der}	NGE	H-DEAN
Fuel	CH_4	CH_4	CH_4	CH_4	CH_4	H_2	H_2
Thrust (lb_f)	25K	40,344	79,366	4,409	25K	25K	44,694
I_{sp} (s)	349.3	378	379	380.6	383	465	429.8
T/W	120.7	44	63	15.5	108	N/A	142.2
Mass (lb_m)	207	917	1260	284	231	N/A	314
M_{prop} (lb_m)	22,323	17,715	17,588	17,388	N/A	N/A	20,600

The mass of propellant for each rocket was calculated for the Δv calculated in chapter 2, 4.3 km/s. The payload mass is assumed as 5000 kg. The f_{inert} estimated for the MDEAN was extended to the other methane rockets. As expected, the MDEAN requires the greatest amount of propellant as it has the lowest I_{sp}. For the MDEAN to have an advantage over the other rockets, the high thrust-to-weight ratio must become an advantage. The weight savings on hardware must be similar to the weight losses due to inferior propellant efficiency. Figure 22 shows the mass of required propellant versus the change in velocity for the methane engines.

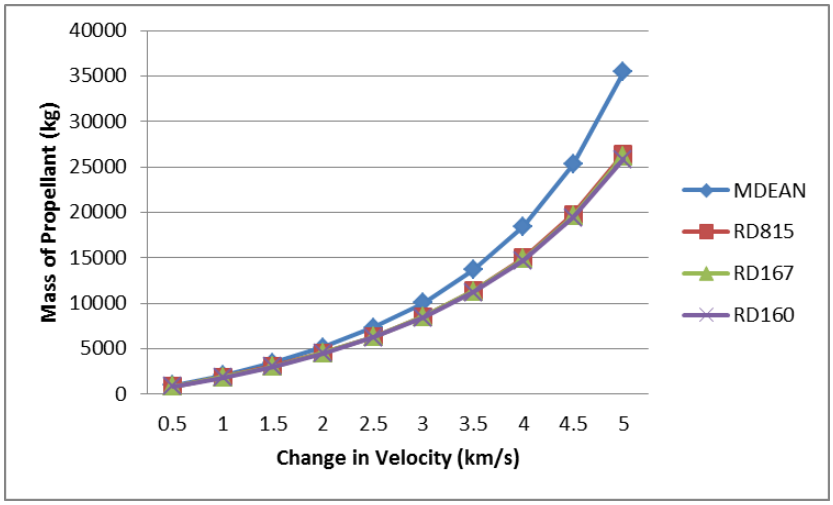

Figure 22: Methane Rockets Propellant Mass Vs. Δv.

It is clear that for any maneuver of significant Δv, I_{sp} is the more important figure of merit. The MDEAN should have a performance advantage over the other methane rockets for a required change in velocity of less than 2 km/s.

One possible benefit of the methane rocket over a similar hydrogen rocket is savings in the mass of the propellant tanks. This comparison is made between Hall's hydrogen DEAN [8] and the MDEAN. The method to estimate the mass of the propellant tanks begins with the change in velocity calculation from chapter 2. The transfer orbit used for the calculation has a Δv requirement of 4.3 km/s. The payload for delivery to orbit is assumed to be 5,000 kg. Next, a f_{inert} is assumed for the rocket stage that is defined by equation 52 [4].

$$f_{inert} = \frac{m_{inert}}{m_{prop} + m_{inert}} \tag{52}$$

where

m_{inert} = Vehicle mass excluding propellant and payload (kg)

m_{prop} = Mass of required propellant (kg)

The mass of propellant can then be calculated by combining the definition of f_{inert} with the ideal rocket equation to reach equation 53.

$$m_{prop} = \frac{\left(e^{\left(\frac{\Delta v}{I_{sp} g_0}\right)} - 1\right)(1 - f_{inert})}{1 - f_{inert} e^{\left(\frac{\Delta v}{I_{sp} g_0}\right)}} \tag{53}$$

With the O/F Ratio, the mass of each propellant can then be calculated. With the total mass of each propellant and the desired thermodynamic state of each storage tank, the density can be determined through the NIST [25, 26] and the volume of the tanks can be calculated. At this point, there are several methods for the calculation for the mass of

cryogenic fluid storage tanks. The tank mass calculation was chosen based on the rule of thumb that the tank weight should be about 5-15% of the propellant weight [29]. The method of tank mass calculation is taken from Humble *et al.* [4]. Once the tanks are sized, a pressurization system mass is estimated, providing the mass of all inert components. This allows for the calculation of f_{inert} and an iterative process to solve for the tank masses. The results of this analysis can be found in Table 25.

Table 25: MDEAN Compared to DEAN.

	MDEAN	**DEAN**
Fuel	**Methane**	**Hydrogen**
m_{engine} (kg)	94	160
m_{prop} (kg)	20,245	23,078
m_{fuel} (kg)	4,764	3,297
$m_{oxidizer}$ (kg)	15,482	19,781
m_{tanks} (kg)	792	2103
m_{inert} (kg)	3067	8,050
$m_{payload}$ (kg)	5,000	5,000
m_{total}, (including payload) (kg)	28,522	35,952

The tank masses were based on spherical tanks of the materials chosen by Hall for the hydrogen (INCOLOY 909) and oxygen (INCONEL 718) feed systems [8]. The mass was calculated by determining the thickness of the tank assuming a safety factor of 2, or a burst pressure of 400 psia. When compared to empirical relationships for cryogenic tanks, all of the tanks are light except for the hydrogen tank, which is significantly heavier. This is not a perfect comparison as the DEAN operates at 50,000 lb_f of thrust while the MDEAN is designed for 25,000 lb_f.

V. Conclusions and Recommendations

This chapter first explores the conclusions and significance of the MDEAN research. Then, based on experience with the model, recommendations for future work are made.

Conclusions of Research

Based on the runs presented in chapter 4, the MDEAN does not represent a significant boost over the state of the art. It does not meet both requirements of 383 seconds of specific impulse with a thrust to weight ratio of over 108. The estimates for all of the simulated methane engines could prove useful to an actual multi stage design. The MDEAN provides an advantage based on volume savings when compared to a hydrogen rocket or a rocket with a bell nozzle. There could be a mission that would favor the characteristics of a MDEAN rocket.

Significance of Research

The MDEAN adds significant capability over the existing DEAN capability. The fluid property tables can be used in other models with some attention to the low temperature methane error. Additionally, this paper outlined the process for exploring different propellants with NPSS. By referencing the methods used for the development of the fluid property tables, it should be possible to develop tables for alternate chemistry in a timely manner.

Additionally, the exploration of an upper stage dual expander aerospike nozzle rocket engine provided a large set of engine mass/performance design data. Given

mission and geometric constraints, it should be possible to query this research to determine if there is a liquid methane/liquid oxygen design concept that would provide a reasonable solution. At the least, it should be possible to deconstruct requirements into a range for the design input variables and explore the solution space.

Recommendations for Future Research

The first several recommendations involve improvements to the existing model. First, the methane Kriging estimator for the fluid property tables requires an improvement. The error at low temperatures should be reduced by including more low temperature data and rebuilding the estimator in ModelCenter. This is a relatively straight forward process, but was not accomplished due to time constraints. Next, the MDEAN should be run over a large set of design input. Because of time constraints, the model was mostly explored over the six input design variables: expansion ratio, throat area, chamber length, characteristic length, oxidizer-to-fuel ratio, and thrust. This design space could be opened up to look at the aspect ratio of the cooling channels, the number of cooling channels, the percent of oxidizer flow through the bypass and more.

Before the design space is fully explored, an upgrade to decrease the time per run of the model should be explored. One opportunity to decrease the time per run is to leave NPSS open from run to run. Currently, for each ModelCenter run, NPSS is opened, ran, and then closed. By just leaving NPSS open from run to run could save significant time over thousands of runs. Averaging over 50 runs, the model takes approximately 8 seconds to complete. Some failure modes within NPSS are on the order of two minutes (not seen in the measured 50 runs), but that is usually because the design point failed to

converge within the limit of iterations. This could and should be improved by reducing the maximum number of iterations from 5000.

A test plan for the model was developed, but not fully executed. More time should be spent on thorough validation and verification. Much of the work on the MDEAN and the concurrently developed DEAN7 was spent on debugging reused code.

More data could be used in several parts of the model. More high temperature methane and oxygen data would provide a better buffer for the cooling channels. Currently, the state of the fluid in the cooling channels can be at a higher temperature than is included in the fluid property tables or the sonic velocity constraint checkers. This is because of a limitation in the available NIST data. More data would prevent this model failure mode, and if a source of thermochemical data is identified, more propellant fluid property tables could be created. Additionally, more material property data as a function of temperature is needed for silicon carbide. The model is currently built around two data points for silicon carbide ultimate tensile strength and yield strength, at 540 R and 1080 R.

NPSS has been advanced to a commercial version of 2.3 while DEAN7 and MDEAN are built with NPSS version 1.65. All NPSS rocket elements would need an upgrade into 2.3, but they should somewhat similar because both versions use a syntax derived from C++. Additionally, the rocket elements could possibly be upgraded to include reacted fluid stations (or new rocket elements could be developed). DEAN only uses unreacted fluid stations and therefore pushed the MDEAN thermochemical solution into using fluid property tables. Several other solution methods exist with different fluid

station types. For example, NPSS can call CEA directly to calculate fluid properties of combustion products, but not with unreacted fluid stations.

Summary

Based on several iterations of a liquid hydrogen and liquid oxygen model built up over years of work, the MDEAN furthers the capability to analyze a diverse selection of rocket concepts. While failing to meet all performance goals derived from the NGE solicitation, the MDEAN yet provides relevant performance estimates to interesting rocket concepts. The final rocket engine concept has an I_{sp} of 349.3 seconds, a thrust-to-weight ratio of 120.7, and a total engine mass of 207.2 lb_m. An examination of this run point demonstrated it is physically realizable.

Appendix A: Simple.mdl

Due to the complexity of the DEAN model, it was undesirable to experiment with changing the fluid property tables. In addition to updating the specified thermodynamics, the fuel pump and the initial guesses of the cooling channel fluid states required update. To reduce the level of complexity of the software update, a simple pressure fed rocket model was developed, *simple.mdl*. Whenever the fluid property tables were updated, they were first tested with the *simple.mdl* model. This allowed for an iterative software update where individual steps of the update could be verified. The model includes propellant tanks, simplified frictional line losses, a rocket combustion chamber, and a rocket nozzle. In addition to the standard independent and dependent variables included with the elements, the following were added:

Table 26: Simple.mdl Independent Variables and Dependent Conditions.

Independent Variables	Dependent Variables
Throat Area	Mass Flow Rate
Chamber Area	Thrust

The solver perturbs the throat area and the chamber area while trying to attain the specified mass flow rate and thrust. The development of this model followed the rocket design process found in Space Propulsion Analysis and Design [4], which provided approximate values of all input variables for the different elements. The performance of the model was not examined as it was simply a tool to test the new fluid property tables independently of other model updates. The code is presented below.

```
//*****************************************************************
    //
    // This is a simple rocket engine.
    // It will serve as a starting point for more detailed models.
```

```
        //
        // 01 Nov 11
        //
//*************************************************************************

        MODELNAME = "Bipropellant";
        string Model_ID = "Methane Oxygen chemical engine";

//*******************************Set Thermochemistry source***************
        setThermoPackage("FPT");

//*****************************Define Input Variables*********************

        real mdot_Ox   = 16.4134;          // O2 fluid mass flow rate (lbm/s)
        real mdot_Fu   = 7.13636;          // Fuel fluid mass flow rate (lbm/s) !!!!!Set to
RP-1 needs adjustment in this model to H2!!!!!!!!!!!!!
        real mdot      = mdot_Ox + mdot_Fu;  // Total mass flow rate (lbm/s)
        real thrust    = 8000.0;           // target thrust (lbf)   7937
        real P_chamber = 101.526;          // chamber pressure (lbf/in2 aka psia)

//*****************************Setup Elements*****************************

        Element Starter TankOx {
            OFR         = 1.0;
            Pt          = 140.0;        // Pressure of ox tank given in psia
            Tt          = 162.0;        // BP of oxygen, storage as liquid at high pressure
deg R
            comp        = "O2_NIST";
        }

        Element Pipe OxPipe {
            Cf          = 100.0;
        }

        Element Starter TankFu {
            OFR         = 0;
            Pt          = 140.0;        // Pressure of ox tank given in psia
            Tt          = 210;          // BP of CH4 (@1atm), but storage as liquid at high
pressure deg R
            comp        = "METHANE";
        //      Tt          = 36;         // BP of CH4 (@1atm), but storage as liquid at high
pressure deg R
        //      comp        = "HYDROGEN";
        }
```

```
        Element Pipe FuPipe {
            Cf          = 100.0;
        }

        Element RocketComb1 Chamber {
            OFR         = 0.75;         // Oxidizer fraction OFR=OF/(1+OF)
            comp        = "C_CH4_O2";     // Composition of hot side gases, only for
combusting H2 and O2
        //      comp        = "C_O2_H2";     // Composition of hot side gases, only for
combusting H2 and O2
            radius_tc   = 6.367;          // Radius of the thrust chamber just before
converging to nozzle (in)
            volume      = 1491.5;       // Volume of gas in chamber, in3
        }

        Element RocketNozzle Nozz {
            AR          = 100.0;         // Area ratio for nozzle exit
            Ath         = 42.09354;      // Area of throat, given in in**2
            Ps          = 0.001;          // Ambient pressure for upper stage, assumed psia
            realLossCoef = 1.0;           // Loss coefficient accounting for everything but
expansion losses (set to default)
            s_Q         = 1.0;           // Scalar on heat transfer rate (set to default)
        }

//*****************************Setup Links**************************

        linkPorts("TankOx.Fl_O",   "OxPipe.Fl_I",     "Ox piping");         //links oxidizer
tank output to a pipe
        linkPorts("OxPipe.Fl_O",   "Chamber.Fl_oxid",  "Fl_oxid_chmbrinput"); //links
oxidizer pipe output to chamber oxidizer input
        linkPorts("TankFu.Fl_O",   "FuPipe.Fl_I",     "Fu piping");         //links fuel tank
output to a pple
        linkPorts("FuPipe.Fl_O",   "Chamber.Fu_I",     "Fl_fuel_chmbrinput"); //links
fuel pipe output to chamber fuel input
        linkPorts("Chamber.Fl_tc", "Nozz.Fl_I",       "Fl_chmbr_to_nozz");   //links
combustion chamber to the nozzle

//*****************************Setup Solver************************
        // Defining output variables
        Chamber.Pt_tc   = P_chamber;
        Chamber.Fl_tc.W = mdot;

        //Initial guesses required for solver initiation
        Chamber.OFR     = 0.75;     //OFR = OF / (1+OF)
        Chamber.Tt_tc   = 5400;     //(R)
```

```
        TankOx.Pt       = 140.0;
        TankOx.Tt       = 162.0;    //(R)
        TankFu.Pt       = 140.0;
        TankFu.Tt       = 210.0;    //(R)
        Chamber.Winj    = mdot;
        Chamber.Fu_I.htRef = 2391.6892; //This is a correction factor to get from NIST
to CEA Enthalpy reference state
        Chamber.Fl_oxid.htRef = 117.0293; //This is a correction factor to get from NIST
to CEA Enthalpy reference state

//Independent Variables
        Independent AThroat {
                varName   = "Nozz.Ath";
                autoSetup = TRUE;
        }

        Independent AChamber {
                varName   = "Chamber.radius_tc";
                autoSetup = TRUE;
        }

//Dependent Variables

        Dependent MassFlow{  //massflow is given in the SPAD description
              eq_lhs    = "Nozz.W";     //solved for in the RocketNozzle Nozz element
              eq_rhs    = "Chamber.Winj";       //provided in the problem statement
              autoSetup = TRUE;
        }

        Dependent Thrust {
              eq_lhs    = "Nozz.Fg";
              eq_rhs    = "thrust";
              autoSetup = TRUE;
        }

        solver.solutionMode = "STEADY_STATE";
        presolverSequence = {};

        autoSolverSetup();
        solver.maxIterations = 100;
        solver.maxJacobians  = 10;
        run ();

        cout << endl;
        cout << endl;
```

```
cout << "   Converged " <<   solver.converged;
cout << endl;
cout << endl;
cout << "   ITT   PASS   JAC  BROY  ";
cout << endl;
cout.width = 6;
cout << solver.iterationCounter
    << solver.passCounter
    << solver.numJacobians
    << solver.numBroydens;
cout << endl;
cout << endl;

cout.width = 4;
//cout.precision = 4;
cout << " Oxygen Tank " ;
cout << "  Pt  "      <<  TankOx.Pt;
cout << "    Tt   "   <<  TankOx.Tt;
cout << endl;

cout << " Fuel Tank   " ;
cout << "  Pt  "      <<  TankFu.Pt;
cout << "    Tt   "   <<  TankFu.Tt;
cout << endl;

cout.precision = 4;
cout.width = 4;
cout << " Ox Pipe     " ;
cout << "Pout "       <<  OxPipe.Fl_O.Pt;
cout << "    hout "       <<  OxPipe.Fl_O.ht;
cout << "    Tout "       <<  OxPipe.Fl_O.Tt;
cout << "    rho_out "       <<  OxPipe.Fl_O.rhot;
cout << "    comp_out "       <<  OxPipe.Fl_O.comp;
cout << "    dp "       <<  OxPipe.dP;
cout << "    ";
cout.width = 4;
//cout.precision = 4;
cout << "      W   "  <<  OxPipe.Fl_O.W;
cout << endl;
cout << " Fu Pipe     " ;
cout.width = 4;
cout.precision = 4;
cout << "Pout "       <<  FuPipe.Fl_O.Pt;
cout << "    hout "       <<  FuPipe.Fl_O.ht;
cout << "    Tout "       <<  FuPipe.Fl_O.Tt;
```

```
cout << "    rho_out "       <<  FuPipe.Fl_O.rhot;
cout << "    comp_out "       <<  FuPipe.Fl_O.comp;
cout << "    dp "       <<  FuPipe.dP;
cout << "             ";
cout.width = 3;
cout.precision = 3;
cout << "      W    "  <<  FuPipe.Fl_O.W;
cout << endl;

cout << " Chamber     " ;
cout.width = 4;
cout.precision = 4;
cout << "  Pt "       <<  Chamber.Pt_tc;
cout << "    Tt   "   <<  Chamber.Tt_tc;
cout.width = 4;
cout.precision = 4;
cout << "    Winj   " <<  Chamber.Winj;
cout << endl;
cout << "          ";
cout << "   Rtc "     <<  Chamber.radius_tc;
cout << "             " ;
cout << "    Wex   "   <<  Chamber.Wnozzle;
cout << endl;
cout << endl;

cout.width = 3;
cout.precision = 3;
cout << " Nozzle     " ;
cout << "   At  "     <<  Nozz.Ath;
cout.width = 5;
cout.precision = 5;
cout << "    Fg  "   <<  Nozz.Fg;
cout.width = 4;
cout.precision = 4;
cout << "    Wnox   "  <<  Nozz.Fl_I.W;
cout << "    Isp   "   <<  Nozz.Isp;
cout << endl;
cout << endl;
```

Appendix B: Software Changes from DEAN7 to MDEAN

This appendix lists the changes that were required to update the standard DEAN model (version 7) to accommodate methane fuel via fluid property tables. The first table outlines the changes to the NPSS model. For these changes to function properly, the fluid property tables must be placed in the following directory in the NPSS folder which is usually installed in the program files directory for a Windows install:

C:\Program Files (x86)\NPSS.nt.V165-OPT-Full\DLMComponents\nt

This will of course change based on the chosen operating system, NPSS version, and file structure. This installation was on Windows 7 with NPSS version 1.65. Note that everything above line 68 of the NPSS model is also controlled through ModelCenter input variables. Variables that are considered design variables are not included in these lists. Changes are also required at the ModelCenter level and are outlined in Table 28.

Table 27: NPSS Updates

Line	Update	Action
22	TargetIsp = 350;	Update to realistic CH4/O2 guessed I_{sp}
25	real T_TankH = 170.0;	Update to realistic CH4 storage temperature
39	real Nmech_RPMF = 50000;	Update to fuel pump rpm based on maintaining specific speed
78	real c_star = 6070;	Update c_star value to 6070 for methane
87	real ht_OCV1 = -62.312;	Update Oxidizer initial enthalpy guesses to NIST thermodynamic basis.
88	real ht_OCV2 = -54.0;	
89	real ht_CVO6 = -52.0;	
90	real ht_CVO5 = -19.0;	
91	real ht_CVO4 = 5.0;	
92	real ht_CVO3 = 27.0;	
93	real ht_CVO2 = 48.0;	
94	real ht_CVO1 = 68.0;	
95	real ht_OCV3 = 68.0;	
96	real ht_TBCV1 = 68.0;	
97	real ht_OCV4 = 59.0;	
99	real ht_HCV1 = -25.243;	Update Fuel initial enthalpy guesses to methane values from the NIST data.
100	real ht_HCV2 = -15.6;	

101	real ht_HCV3 = 65.95;	
102	real ht_CVH8 = 111.7;	
103	real ht_CVH7 = 221.2;	
104	real ht_CVH6 = 226.7;	
105	real ht_CVH5 = 328.1;	
106	real ht_CVH4 = 388.6;	
107	real ht_CVH3 = 439.6;	
108	real ht_CVH2 = 485.99;	
109	real ht_CVH1 = 532.1;	
110	real ht_HCV4 = 532.1;	
111	real ht_HCV5 = 440.6;	
125	real rho_HD1 = 27.89;	Update to initial methane guesses for density.
126	real rho_DuctH8 = 22.5;	
127	real rho_DuctH7 = 19.82;	
128	real rho_DuctH6 = 16.116;	
129	real rho_DuctH5 = 13.6688;	
130	real rho_DuctH4 = 10.45;	
131	real rho_DuctH3 = 8.829;	
132	real rho_DuctH2 = 7.524;	
133	real rho_DuctH1 = 6.649;	
134	real rho_TBH0 = 6.66;	
135	real rho_HV = 4.43299;	
537	setThermoPackage("FPT");	Specifies new thermodynamic package
542	setDefaultComposition("C_CH4_O2");	For the chamber and nozzle, the composition is the combustion products unless otherwise specified. This calls the fluid property table named: C_CH4_O2.fpt
544	comp = "C_CH4_O2";	Specifies combustion products for combustion chamber exit port, redundant to line 542, but original NPSS model included it.
547	Fu_I.comp = "METHANE";	Specifies METHANE.fpt fluid property table.
548	Fl_oxid.comp = "O2_NIST";	Specifies O2_NIST.fpt fluid property table.
636	setDefaultComposition("O2_NIST");	Specifies O2_NIST.fpt fluid property table for all flow stations until new composition is specified.
859	setDefaultComposition("METHANE");	Specifies METHANE.fpt fluid property table for all flow stations until new composition is specified.
1287	COMB.Fu_I.htRef = 2391.6892;	Added correction factor to convert from NIST thermodynamic enthalpy basis to CEA enthalpy basis for methane.
1288	COMB.Fl_oxid.htRef = 117.0293;	Added correction factor to convert from NIST thermodynamic enthalpy basis to CEA enthalpy basis for oxygen.

Table 28: ModelCenter Updates.

Component	Update	Action
DesignVariables.Materials	Spike_Cool_Mat = Silicon Carbide	Change the aerospike side cooling jacket to silicon carbide as the copper melts.
TargetIsp	Change to 350	Redundant to NPSS change, but necessary if NPSS model is to be used independent of ModelCenter
DEAN	T_TankHNmech_RPMF	Change thse values to match the NPSS input values for consistency.
Constraints.LH2.LH2_Machs.SonVel_H2	Methane Kriging Sonic Velocity estimator	Replace H2 SonVel estimator with CH4 SonVel estimator.
Performance.CEA	Different Component that selects correct fuel	Updated with different wrapper.

Bibliography

1. LeMay Center/DD. *AFDD 3-14 Space Operations*. Retrieved September 7, 2011, from Curtis E. Lemay Center for Doctrine Development and Education: http://www.au.af.mil/au/lemay/main.htm, 27 November 2006.

2. Futron Corporation. *Space Transportation Costs: Trends in Price Per Pound to Orbit 1990-2000*. Retrieved September 7, 2011, from: http://www.futron.com/upload/wysiwyg/Resources/Whitepapers/Space_Transportation_Costs_Trends_0902.pdf, 6 September 2002.

3. Chemical Economics Handbook, SRI – October 2007 http://www.hydrogenambassadors.com/background/worldwide-hydrogen-production-analysis.php

4. Humble, R. H. *Space Propulsion Analysis and Design*. McGraw-Hill, 1995

5. United States Air Force. Retrieved September 7, 2011, from https://www.fbo.gov/index?s=opportunity&mode=form&id=d23c8a2ed2c27f3ce252c6e702a89a10&tab=core&_cview=0, 27 September 2010.

6. Klepikov, I. K. "The new generation of rocket engines, operating by ecologically safe propellant "liquid oxygen and liquefied natural gas(methane)."" *Acta Astronautica*, 209-217, 1997.

7. Sutton, G. P. *Rocket Propulsion Elements, 8th Edition.* Hoboken, NJ: John Wiley & Sons, 2010.

8. Hall, J. *Optimized Dual Expander Aerospike Rocket*. MS Thesis, AFIT/GAE/ENY/11-M10. Graduate School of Engineering and Management, Air Force Institute of Technology (AU), Wright-Patterson AFB OH, March 2011.

9. Arguello, M. *The Concept Design of a Split Flow Liquid Hydrogen Turbopump*. MS Thesis, AFIT/GAE/ENY/08-M01. Graduate School of Engineering and Management, Air Force Institute of Technology (AU), Wright-Patterson AFB OH, 2008.

10. Strain, M. *Design of an Oxygen Turbopump for a Dual Expander Cycle Rocket Engine*. MS Thesis, AFIT/GAE/ENY/08-M26. Graduate School of Engineering and Management, Air Force Institute of Technology (AU), Wright-Patterson AFB OH, 2008.

11. Huzel, D. K. *Modern Engineering for Design of Liquid-Propellant Rocket Engines.* Washington DC: American Institute of Aeronautics and Astronautics, Inc, 1992.

12. Turns, S. R. *An Introduction to Combustion. Second Edition.* McGraw-Hill, 2000.

13. Martin, D. *Computational Design of Upperstage Chamber, Aerospike, and Cooling Jacket for Dual-Expander Rocket Engine*. MS Thesis AFIT/GAE/ENY/11-M10. Graduate School of Engineering and Management, Air Force Institute of Technology (AU), Wright-Patterson AFB OH, 2008.

14. Simmons, J. *Parametric Study of Dual-Expander Aerospike Nozzle Engine*. JANNAF Conference, May 2010.

15. Guernsey, Carl S., Raymond S. Baker, David Plachta, Co-Investigator, Dr. Peter Kittel, Robert J. Christie, and John Jurns, "*Cryogenic Propulsion With Zero Boil-Off Storage Applied to Outer Planetary Exploration*," Final Report, April 8, 2005, (JPL D-31783).

16. Lide, D. R. *CRC Handbook Chemistry and Physics 80th Edition.* CRC Press, 1999.

17. Bohling, Geoff. Lecture Notes, *C&PE 940, Kriging*. Kansas Geological Survey. http://people.ku.edu/~gbohling/cpe940/Kriging.pdf, 19 October 2005.

18. NPSS Rockets Supplement. Software Release: NPSS_1.6.5. Doc. #: NPSS-Rockets. NASA John H. Glenn Research Center at Lewis Field, 12 March 2008.

19. NPSS User Guide. Software Release: NPSS_2.2.1. Doc. #: NPSS-User. Numerical Propulsion System Simulation Consortium. http://npssconsortium.org/members/docs/UserGuide.htm#_Toc238529721, 10 August 2009.

20. Gordon, Sanford and McBride, Bonnie J. *Computer Program for Calculation of Complex Chemical Equilibrium Compositions and Applications: II. Users Manual and Program Description*. NASA Reference Publication 1311, June 1996.

21. Gordon, Sanford and McBride, Bonnie J. *Computer Program for Calculation of Complex Chemical Equilibrium Compositions and Applications: I. Analysis*. NASA Reference Publication 1311, October 1994.

22. Numerical Propulsion System Simulation Consortium. *NPSS Thermodynamic Property Package Reference Sheets. Software Release: NPSS_2.3. Doc. #: NPSS-Thermo.* http://npssconsortium.org/members/docs/NPSS_ThermoPackageRefSheets.htm, 15 February 2010.

23. E.W. Lemmon, M.O. McLinden and D.G. Friend. "Thermophysical Properties of Fluid Systems." in NIST Chemistry WebBook, NIST Standard Reference

Database Number 69, Eds. P.J. Linstrom and W.G. Mallard, National Institute of Standards and Technology, Gaithersburg MD, 20899, http://webbook.nist.gov, 2012.

24. Tannehill, John C. Anderson, Dale A. Pletcher, Richard H. *Computational Fluid Mechanics and Heat Transfer, Second Edition*. Washington D.C.: Taylor and Francis, 1997.

25. Brower, G.T.; Thodos, G.,Vapor Pressures of Liquid Oxygen Between the Triple Point and Critical Point, J. Chem. Eng. Data, 1968, 13, 2, 262-264. Via NIST: http://webbook.nist.gov/cgi/cbook.cgi?ID=C7782447&Units=SI&Mask=4#Thermo-Phase, 2012.

26. Prydz, R.; Goodwin, R.D., Experimental Melting and Vapor Pressures of Methane, J. Chem. Thermodyn., 1972, 4, 127-133. Via NIST: http://webbook.nist.gov/cgi/cbook.cgi?ID=C74828&Units=SI&Mask=4#Thermo-Phase

27. Haidn, O.J. Advanced Rocket Engines. In *Advances on Propulsion Technology for High-Speed Aircraft* (pp. 6-1 – 6-40). Educational Notes RTO-EN-AVT-150, Paper 6. Neuilly-sur-Seine, France: RTO. Available from: http://www.rto.nato.int, 2008.

28. Atkins, Peter. *Physical Chemistry*. New York: W.H. Freeman and Company, 1998.

29. Wertz, James R. and Larson, Wiley J. *Space Mission Analysis and Design*. Hawthorne, CA: Microcosm Press and New York: Springer, 1999.

Vita

Captain Michael D. Moen graduated with the class of 2001 from The University of Texas at Austin earning a Bachelor of Science in Chemical Engineering. After commissioning through Officer Training School, he researched gas lasers with the Air Force Research Laboratory at Kirtland Air Force Base. Following an assignment with the C-130 Avionics Modernization Program, he was selected for the Astronautical Engineering master's program at the Air Force Institute of Technology. His studies included a focus on space propulsion. Upon graduation in 2012, he will move to his next assignment with the Space Development and Test Directorate at Kirtland Air Force Base, New Mexico.

REPORT DOCUMENTATION PAGE

Form Approved
OMB No. 074-0188

PLEASE DO NOT RETURN YOUR FORM TO THE ABOVE ADDRESS.

1. REPORT DATE *(DD-MM-YYYY)*	2. REPORT TYPE	3. DATES COVERED *(From – To)*
22-03-2012	Master's Thesis	22-05-2010 – 22-03-2012

4. TITLE AND SUBTITLE
Methane Dual Expander Aerospike Nozzle Rocket Engine

5a. CONTRACT NUMBER

5b. GRANT NUMBER

5c. PROGRAM ELEMENT NUMBER

6. AUTHOR(S)
Moen, Michael D., Capt, USAF

5d. PROJECT NUMBER
N/A

5e. TASK NUMBER

5f. WORK UNIT NUMBER

7. PERFORMING ORGANIZATION NAMES(S) AND ADDRESS(S)
Air Force Institute of Technology
Graduate School of Engineering and Management (AFIT/ENV)
2950 Hobson Way, Building 640
WPAFB OH 45433-8865

8. PERFORMING ORGANIZATION REPORT NUMBER
AFIT/GA/ENY/12-M12

9. SPONSORING/MONITORING AGENCY NAME(S) AND ADDRESS(ES)
Dr. Richard K. Cohn (richard.cohn@edwards.af.mil)Air Force Research LaboratoryAFRL/RZSE; Bldg 8351, Rm 118B; Edwards AFB, CA 93524
DSN: 525-6177 Comm: (661) 275-6177

10. SPONSOR/MONITOR'S ACRONYM(S)

11. SPONSOR/MONITOR'S REPORT NUMBER(S)

12. DISTRIBUTION/AVAILABILITY STATEMENT
APPROVED FOR PUBLIC RELEASE; DISTRIBUTION UNLIMITED

13. SUPPLEMENTARY NOTES
This material is declared a work of the United States Government and is not subject to copyright protection in the United States.

14. ABSTRACT
The Air Force Institute of Technology (AFIT), working to meet requirements set by the Air Force Research Laboratory's Next Generation Engine (NGE) initiative, is developing upper stage rocket models. The current path of investigation focuses on combining a dual expander cycle with an aerospike nozzle, or the Dual Expander Aerospike Nozzle (DEAN) using methane fuel. The design process will rely heavily on AFIT's previous work, which focused on the development of tools for and the optimization of a hydrogen/oxygen DEAN engine. The work outlined in this paper expands the existing research by substituting methane for hydrogen. The targets derived from the NGE program include a vacuum specific impulse of 383 seconds, 25,000 lbf of thrust, and a thrust to weight ratio of 108. NASA's Numerical Propulsion System Simulation was used in conjunction with Phoenix Integration's ModelCenter to optimize over several parameters to include O/F ratio, thrust, and engine geometry. After thousands of iterations over the design space, the selected MDEAN engine concept has 349 s of Isp and a thrust to weight ratio of 120. The MDEAN was compared to liquid hydrogen technology, existing methane technology, and the NGE goals.

15. SUBJECT TERMS
Rocket, Engine, Methane, Aerospike

16. SECURITY CLASSIFICATION OF:			17. LIMITATION OF ABSTRACT	18. NUMBER OF PAGES	19a. NAME OF RESPONSIBLE PERSON
a. REPORT	b. ABSTRACT	c. THIS PAGE			Hartsfield, Carl R., Lt Col, Ph.D, USAF
U	U	U	UU	130	19b. TELEPHONE NUMBER *(Include area code)* (937) 255-6565, x 7472 (carl.hartsfield@afit.edu)

Standard Form 298 (Rev. 8-98)
Prescribed by ANSI Std. Z39-18